Electronic Supplementary Material (ESI) for Journal of Materials Chemistry A.

Remarkable iodine uptake by aniline-based macrocyclic arenes through a reverse dissolution mechanism

Pengyue Jin,[a] Wenting Liang,[b] Yanqin Rong,[a] Wuanhua Wu,*[a] Min Gou,*[a] Yueqin Tang,[a] and Cheng Yang*[a]

[a]. Key Laboratory of Green Chemistry & Technology of Ministry of Education, College of Chemistry, State Key Laboratory of Biotherapy, and College of Architecture and Environment, Sichuan University, Chengdu 610064, China.

[b]. Institute of Environmental Science, & Department of Chemistry, Shanxi University, Taiyuan 030006, China.

Supplemental Experimental Procedures

Table of Contents

1. Materials and methods

All reagents were purchased commercially and used without further purification unless otherwise noted. Iodine (99.99%) was purchased from Adamas-beta Chemical Company. ^{1}H and ^{13}C NMR spectra were recorded at room temperature on a Bruker AMX-400 (operating at 400 MHz for ^{1}H NMR and 101 MHz for ^{13}C NMR) with TMS as the internal standard. HRMS data were measured with a Waters-Q-TOF Premiers (ESI) spectrometer. UV-vis spectra were recorded by using a JASCO V650 spectrometer. Fluorescence spectra were taken on a JASCO FP-8500 spectrofluorometer, and the bandwidth for the measurement was not fixed. Fourier transform infrared (FT-IR) spectroscopy measurements were performed on a Bruker Tensor 27 spectrophotometer. Thermogravimetric Analysis (TGA) was recorded using a DTG-60 instrument or TA Instruments Q50, and the samples were heated under a flowing nitrogen atmosphere at a rate of 10 °C/min. Powder X-ray diffraction (PXRD) data were measured with a powder X-ray diffractometer (X' Pert Pro MPD DY129) at a range of 5-60° of 2θ. Field emission scanning electron microscope(FESEM) and energy-dispersive spectroscopy (EDS) investigations were carried out on Thermo Scientific Apreo 2C. X-ray photoelectron spectroscopy (XPS) was obtained on a Thermo Fisher ESCALAB 250Xi. N_2 adsorption isotherms measurements were performed with a QUANTACHROME instrument at 77.35 K

2. Synthesis and characterizations of An[2]s and P-Ns

Synthesis of Ans

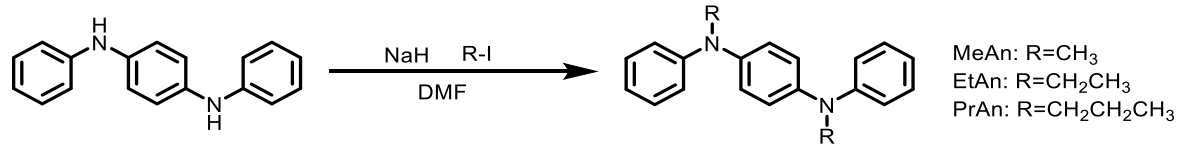

MeAn: N,N'-Diphenyl-p-phenylenediamine (5.23 g, 20 mmol) and NaH (2.4 g ,100 mmol) were added in 100 mL of DMF in an ice bath. After stirring for 30 min, 4 mL CH_3I was added to the reaction mixture, and the reaction mixture was stirred under an N_2 atmosphere at room temperature for additional 4 h until the reaction was completed (as monitored by TLC). 100 mL water was added, and brown precipitate was collected by filtration. The solid was washed with water 3 times and dissolved in ethyl acetate. The organic phase was dried over Na_2SO_4, and the solvent was removed under reduced pressure. The residue was purified by silica gel column chromatography (PE:DCM = 2:1) to afford **MeAn** as a yellow solid (5.17 g**,** 89.7**%**). ^{1}H NMR (400 MHz, $CDCl_3$) δ 7.26 (dd, *J* = 8.6, 7.3 Hz, 4H), 7.04 (s, 4H), 6.97 (s, 4H), 6.89 (t, *J* = 7.3 Hz, 2H), 3.31 (s, 6H). ^{13}C NMR (101 MHz, $CDCl_3$) δ 149.4, 143.9, 129.1, 123.3, 119.9, 118.3, 40.4. HRMS (ESI) m/z calcd for $C_{20}H_{20}N_2$: 288.1627 [M]; found: 288.1654. m.p. 156.4-156.6 °C

EtAn: N,N'-Diphenyl-p-phenylenediamine (5.23 g, 20 mmol) and NaH (2.4 g ,100 mmol) were added in 100 mL of DMF in an ice bath. After stirring for 30 min, 4.68 mL CH_3CH_2I was added to the reaction mixture, and the reaction mixture was stirred under an N_2 atmosphere at room temperature for additional 4 h until the reaction was completed. 100 mL water was added, and brown precipitate was collected by filtration. The solid was washed with water 3 times and dissolved in ethyl acetate. The organic phase was dried over Na_2SO_4, and the solvent was removed under reduced pressure. The residue was purified by silica gel column chromatography (PE:DCM = 3:1) to afford **EtAn** as a yellow solid (5.45 g, 86.3**%**).^{1}H NMR (400 MHz, $CDCl_3$) δ 7.54 – 7.47 (m, 4H), 7.26 (s, 4H), 7.23 – 7.15 (m, 4H), 7.13 (ddt, *J* = 8.4, 7.4, 1.1 Hz, 2H), 4.02 (q, *J* = 7.1 Hz, 4H), 1.50 (dd, *J* = 9.3, 4.9 Hz, 6H). ^{13}C NMR (101 MHz, $CDCl_3$) δ 148.2, 142.8, 129.2, 124.1, 119.5, 118.5, 46.5, 12.75. HRMS (ESI) m/z calcd for $C_{22}H_{24}N_2$: 316.1940 [M]; found: 316.1984. m.p. 99.2-99.4 °C

PrAn: N,N'-Diphenyl-p-phenylenediamine (5.23 g, 20 mmol) and NaH (2.4 g ,100 mmol) were added in 100 mL of DMF in an ice bath. After stirring for 30 min, 5.83 mL $CH_3CH_2CH_2I$ was to the reaction mixture, and the reaction mixture was stirred under an N_2 atmosphere at room temperature for additional 4 h until the reaction was completed. 100 mL water was added, and brown precipitate was collected by filtration. The solid was washed with water 3 times and dissolved in ethyl acetate. The organic phase was dried over Na_2SO_4, and the solvent was removed under reduced pressure. The residue was purified by silica gel column chromatography (PE:DCM = 3:1) to afford **PrAn** as a yellow solid (6.13 g, 89.2%). ^{1}H NMR (400 MHz, $CDCl_3$) δ 7.54 – 7.48 (m, 4H), 7.26 (s, 4H), 7.19 (d, *J* = 7.8 Hz, 4H), 7.13 (t, *J* = 7.3 Hz, 2H), 3.97 – 3.82 (m, 4H), 2.03 – 1.93 (m, 4H), 1.23 (t, *J* = 7.4 Hz, 6H). ^{13}C NMR (101 MHz, $CDCl_3$) δ 148.5, 142.6, 129.1, 124.1, 119.5, 118.5, 54.2, 20.7, 11.4. HRMS (ESI) m/z calcd for $C_{24}H_{28}N_2$: 344.2253 [M]; found: 344.2268. m.p. 84.1-84.2 °C

Synthesis of An[2]s

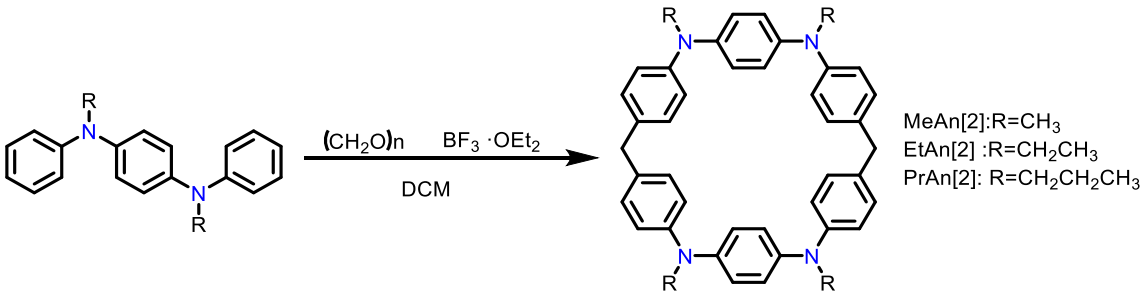

MeAn[2]: MeAn (2.88 g,10 mmol) and paraformaldehyde (900 mg, 30 mmol) were added in 300 mL dichloromethane. After the suspension was stirred at 25 °C for 30 min, $BF_3{\cdot}OEt_2$ (1.2 mL, 10 mmol) was added. The reaction mixture was stirred at room temperature for 24 h, and then quenched by the addition of water. The precipitate was collected by filtration and washed with ethyl acetate to give a dark blue solid which is the linear polymer P-A. The organic phase was washed with saturated aqueous $NaHCO_3$, H_2O, and brine and dried over Na_2SO_4. After the solvent was removed under reduced pressure, the residue was subjected to silica gel column chromatography (PE:EA = 8:1) to give **MeAn[2]** as a white solid (1.21 g, 40.12%). ^{1}H NMR (400 MHz, $CDCl_3$) δ 7.02 (d, *J* = 8.5 Hz, 8H), 6.89 (d, *J* = 8.5 Hz, 8H), 6.80 (s, 8H), 3.83 (s, 4H), 3.23 (s, 12H). ^{13}C NMR (101 MHz, $CDCl_3$) δ 147.5, 143.9, 134.9, 129.4, 121.3, 120.5, 49.5, 40.5. HRMS (ESI) m/z calcd for $C_{42}H_{40}N_4$: 600.3253 [M]; found: 600.3291. m.p. >300 °C

EtAn[2]: EtAn (3.16 g,10 mmol) and paraformaldehyde (900 mg, 30 mmol) were added in 300 mL dichloromethane. After the suspension was stirred at 25 °C for 30 min, $BF_3{\cdot}OEt_2$ (1.2 mL, 10 mmol) was added. The reaction mixture was stirred at room temperature for 24 h, and then quenched by the addition of water. The precipitate was collected by filtration and washed with ethyl acetate to give a dark blue solid which is the linear polymer P-B. The organic phase was washed with saturated aqueous $NaHCO_3$, H_2O, and brine and dried over Na_2SO_4. After the solvent was removed under reduced pressure, the residue was subjected to silica gel column chromatography (PE: EA =10 :1) to afford **EtAn[2]** as a white solid(1.43g, 43.56%). ^{1}H NMR (400 MHz, $CDCl_3$) δ 6.99 (d, *J* = 8.5 Hz, 8H), 6.86 (t, *J* = 6.6 Hz, 8H), 6.75 (s, 8H), 3.82 (s, 4H), 3.68 (q, *J* = 7.0 Hz, 8H), 1.17 (t, *J* = 7.1 Hz, 12H). ^{13}C NMR (101 MHz, $CDCl_3$) δ 146.1, 142.2, 134.5, 129.5, 121.8, 121.0, 46.4, 40.4, 12.8. HRMS (ESI) m/z calcd for $C_{46}H_{48}N_4$: 656.3879 [M]; found: 656.3905. m.p. >300 °C

PrAn[2]: PrAn (3.44 g,10 mmol) and paraformaldehyde (900 mg, 30 mmol) were added in 300 mL dichloromethane. After the suspension was stirred at 25 °C for 30 min, $BF_3{\cdot}OEt_2$ (1.2 mL, 10 mmol) was added. The reaction mixture was stirred at room temperature for 24 h, and then quenched by the addition of water. The precipitate was collected by filtration and washed with ethyl acetate to give a dark blue solid which is the linear polymer P-C. The organic phase was washed with saturated aqueous $NaHCO_3$, H_2O, and brine and dried over Na_2SO_4. After the solvent was removed under reduced pressure, the residue was subjected to silica gel column chromatography (PE:EA = 12 :1) to afford **PrAn[2]** as a white solid(1.62 g, 45.49%) . ^{1}H NMR (400 MHz, $CDCl_3$) δ 7.01 (d, *J* = 8.5 Hz, 8H), 6.90 – 6.84 (m, 8H), 6.76 (s, 8H), 3.84 (s, 4H), 3.62 – 3.54 (m, 8H), 1.71 – 1.61 (m, 8H), 0.93 (t, *J* = 7.4 Hz, 12H). ^{13}C NMR (101 MHz, $CDCl_3$) δ 146.5, 142.6, 134.4, 129.5, 121.8, 121.0, 54.1, 40.3, 20.7, 11.5. HRMS (ESI) m/z calcd for $C_{50}H_{56}N_4$: 712.4505 [M]; found: 712.3437. m.p. >300 °C.

Table S1. Synthesis of **MeAn[2]** under different conditions.

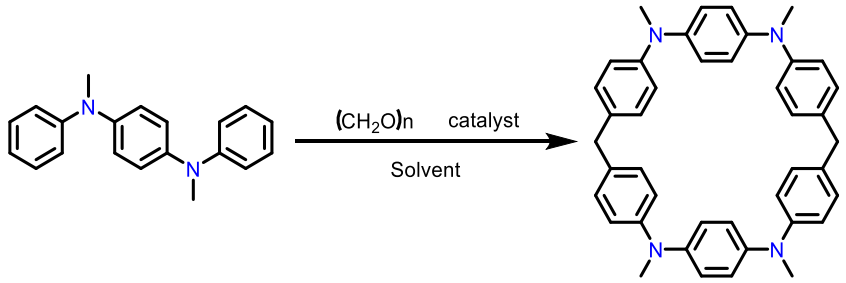

entry	solvent	catalyst	$\frac{[\text{catalyst}]}{[\text{MeAn}]}$	template	Time/h	Yield(%)
1	dichloromethane	$BF_3{\cdot}OEt_2$	1 eq.		6	15%
2	dichloromethane	$BF_3{\cdot}OEt_2$	1 eq.		12	20%
3	dichloromethane	$BF_3{\cdot}OEt_2$	1 eq.		**24**	**40%**
4	dichloromethane	$BF_3{\cdot}OEt_2$	1 eq.		36	35%
5	dichloromethane	$BF_3{\cdot}OEt_2$	1 eq.	1 eq I_2	36	36%
6	dichloromethane	$BF_3{\cdot}OEt_2$	1 eq.	1 eq KI	36	38%
7	dichloromethane	$BF_3{\cdot}OEt_2$	0.1 eq.		24	<1%
8	dichloromethane	$BF_3{\cdot}OEt_2$	0.5 eq.		24	10%
9	dichloromethane	$BF_3{\cdot}OEt_2$	2 eq.		24	5%
10	dichloromethane	$BF_3{\cdot}OEt_2$	5 eq.		24	2%
11	1,2-dichloroethane	$BF_3{\cdot}OEt_2$	1 eq.		12	5%
12	1,2-dichloroethane	$BF_3{\cdot}OEt_2$	1 eq.		24	20%
13	Chloroform	BF3·OEt2	1 eq.		12	10%
14	Chloroform	BF3·OEt2	1 eq.		24	25%
15	dichloromethane	H_2SO_4	1 eq.		24	<1%
16	dichloromethane	TFA	1 eq.		24	<1%
17	dichloromethane	TsOH	1 eq.		24	<1%
18	dichloromethane	$FeCl_3$	1 eq.		24	<1%
20	dichloromethane	$FeCl_3{\cdot}6H_2O$	1 eq.		24	<1%
21	dichloromethane	$AlCl_3$	1 eq.		24	<1%

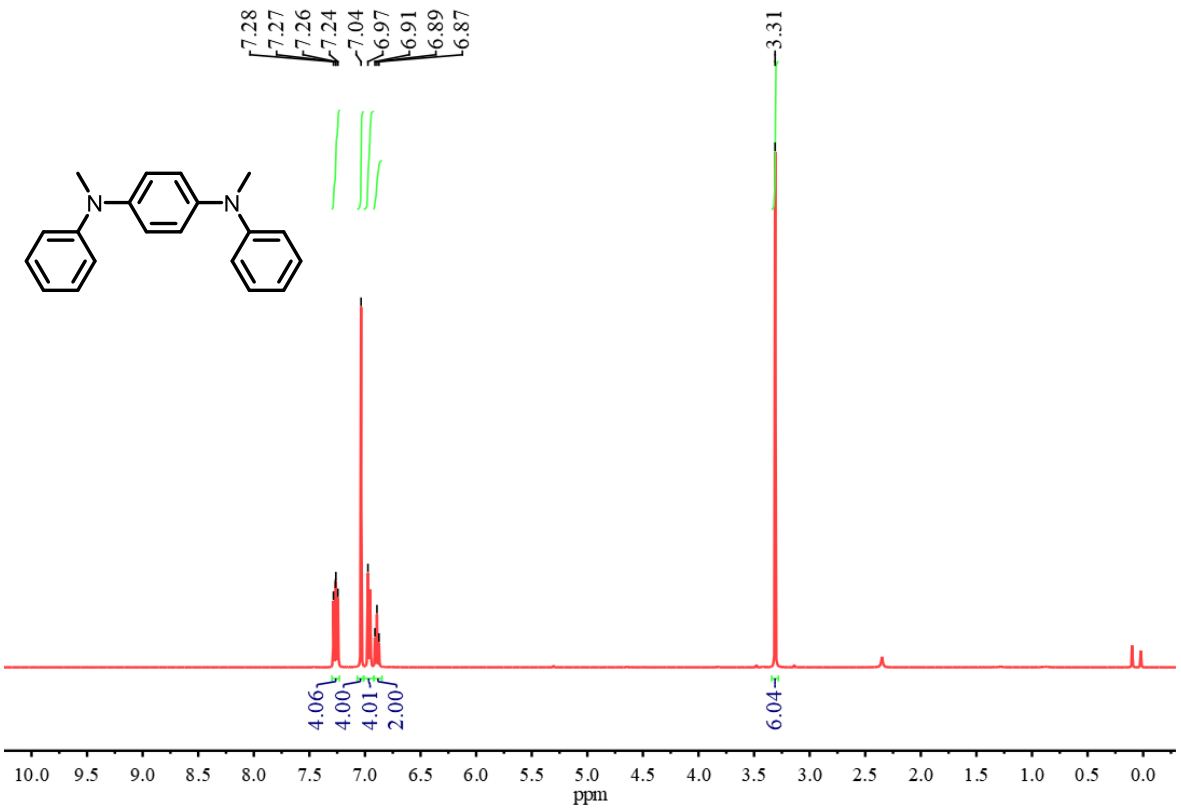

Fig. S1. ^{1}H NMR spectrum of **MeAn** measured in $CDCl_3$ at 25 °C.

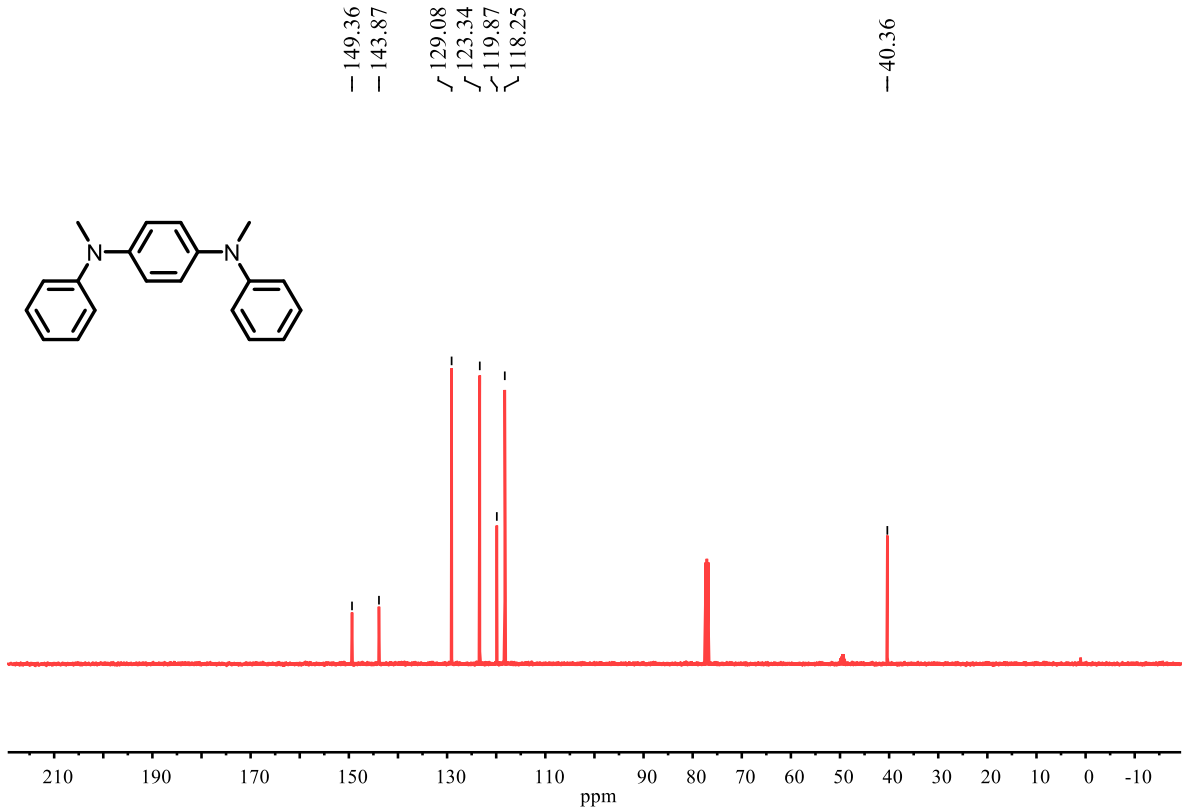

Fig. S2. ^{13}C NMR spectrum of **MeAn** measured in $CDCl_3$ at 25 °C.

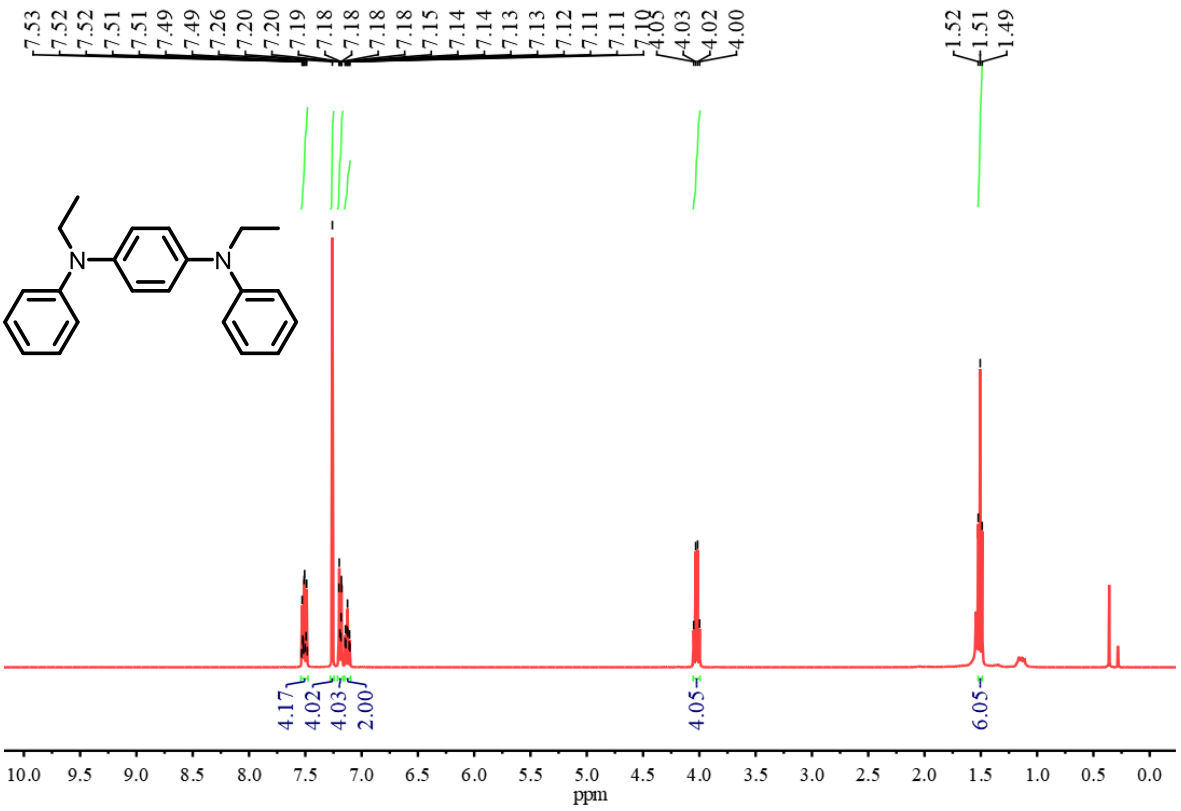

Fig. S3. ^{1}H NMR spectrum of **EtAn** measured in $CDCl_3$ at 25 °C

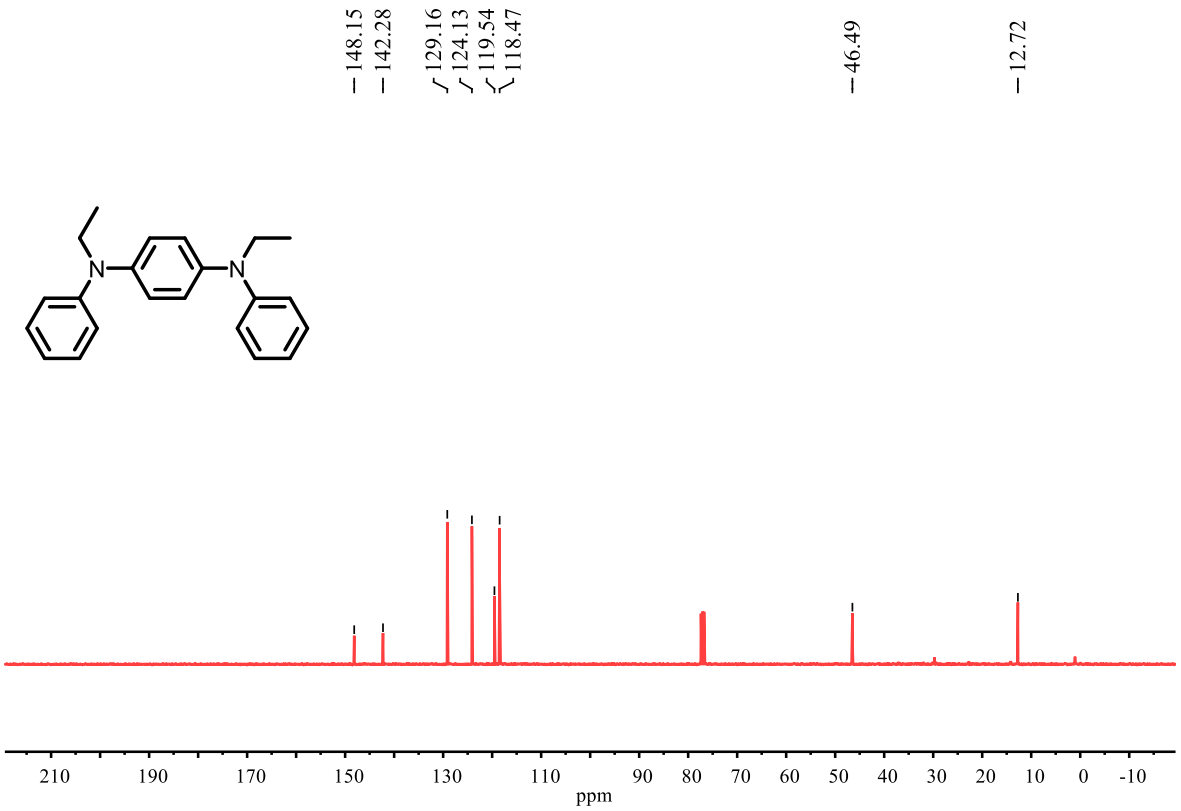

Fig. S4. ^{13}C NMR spectrum of **EtAn** measured in $CDCl_3$ at 25 °C.

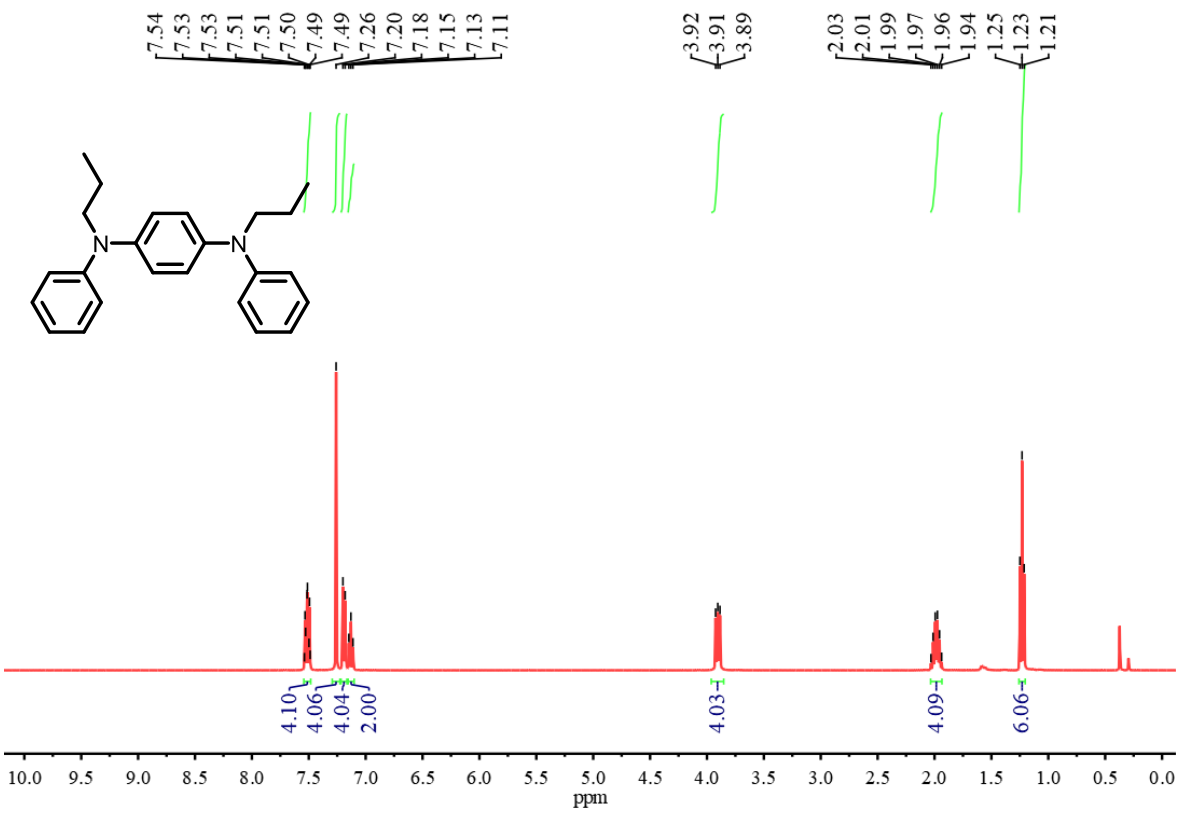

Fig. S5. ^{1}H NMR spectrum of **PrAn** measured in $CDCl_3$ at 25 °C.

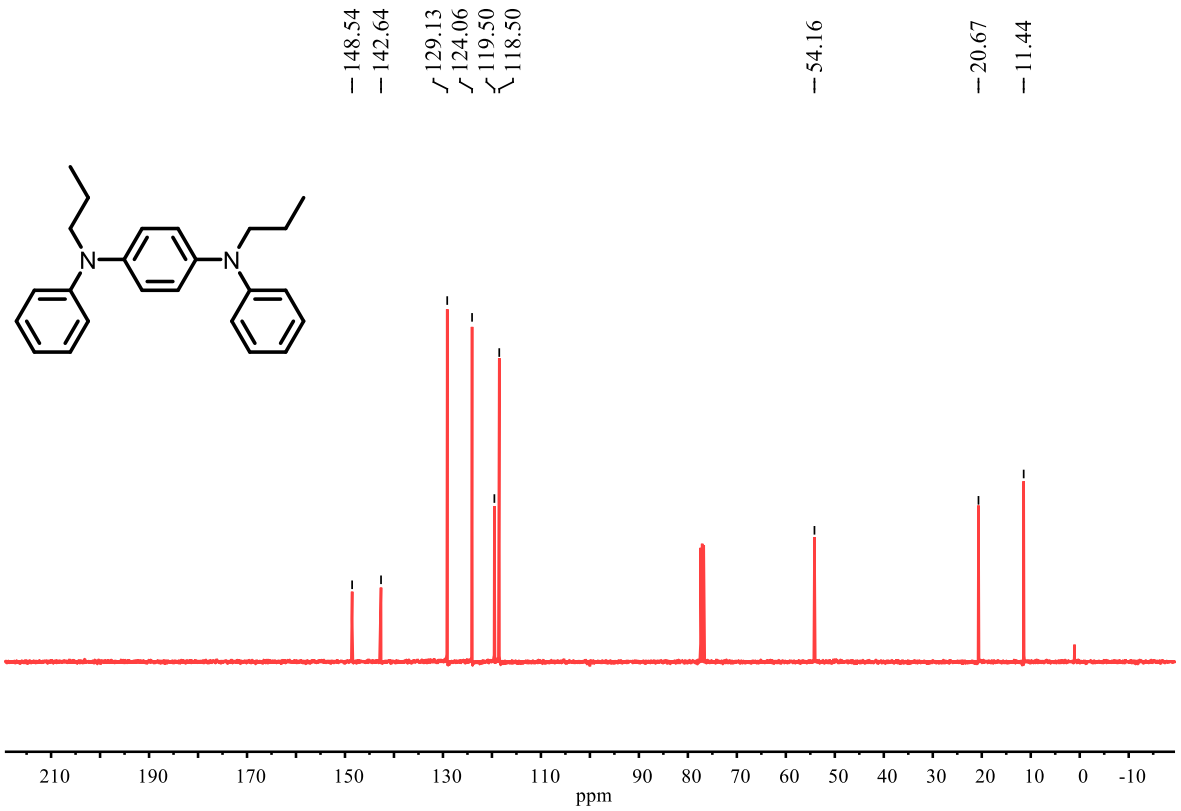

Fig. S6. ^{13}C NMR spectrum of **PrAn** measured in $CDCl_3$ at 25 °C.

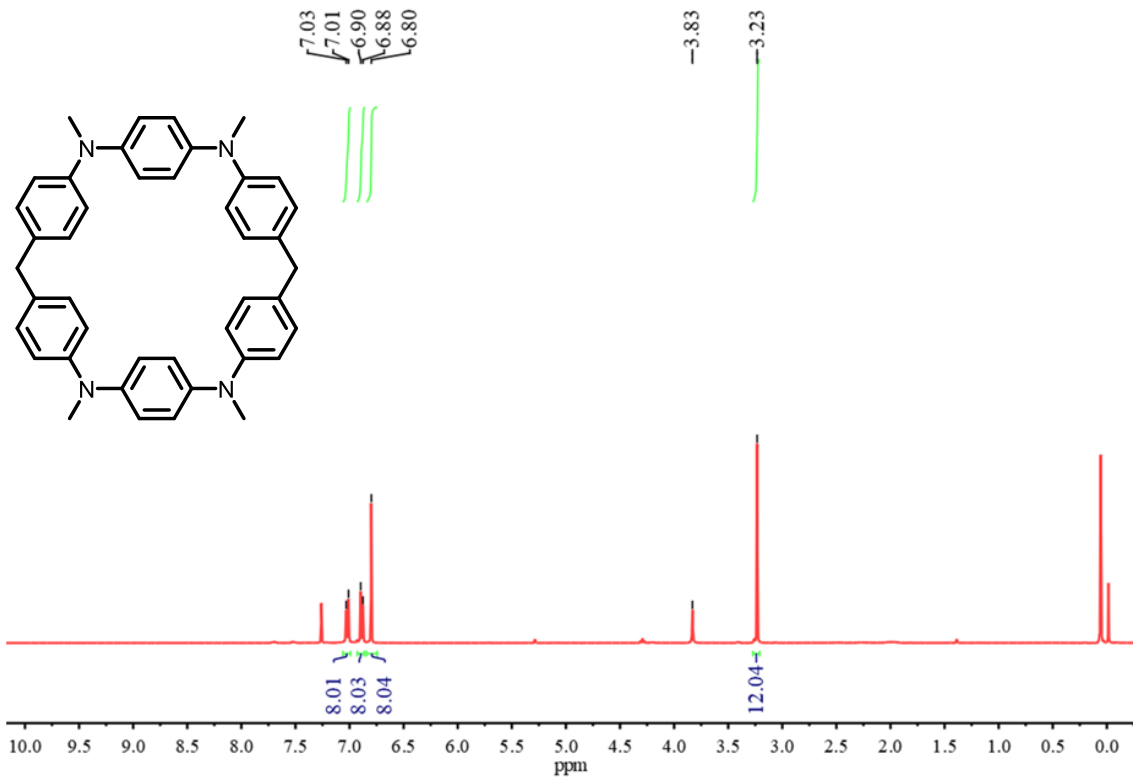

Fig. S7. ^{1}H NMR spectrum of **MeAn[2]** measured in $CDCl_3$ at 25 °C.

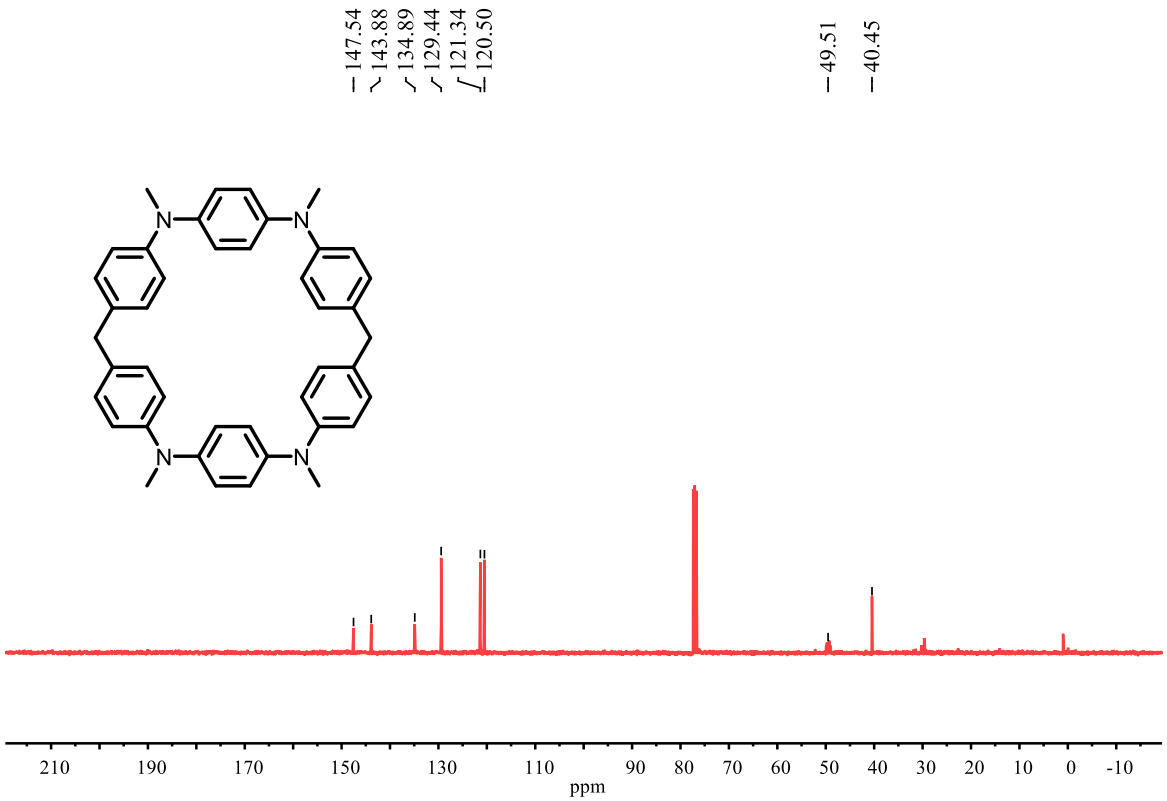

Fig. S8. ^{13}C NMR spectrum of **MeAn[2]** measured in $CDCl_3$ at 25 °C.

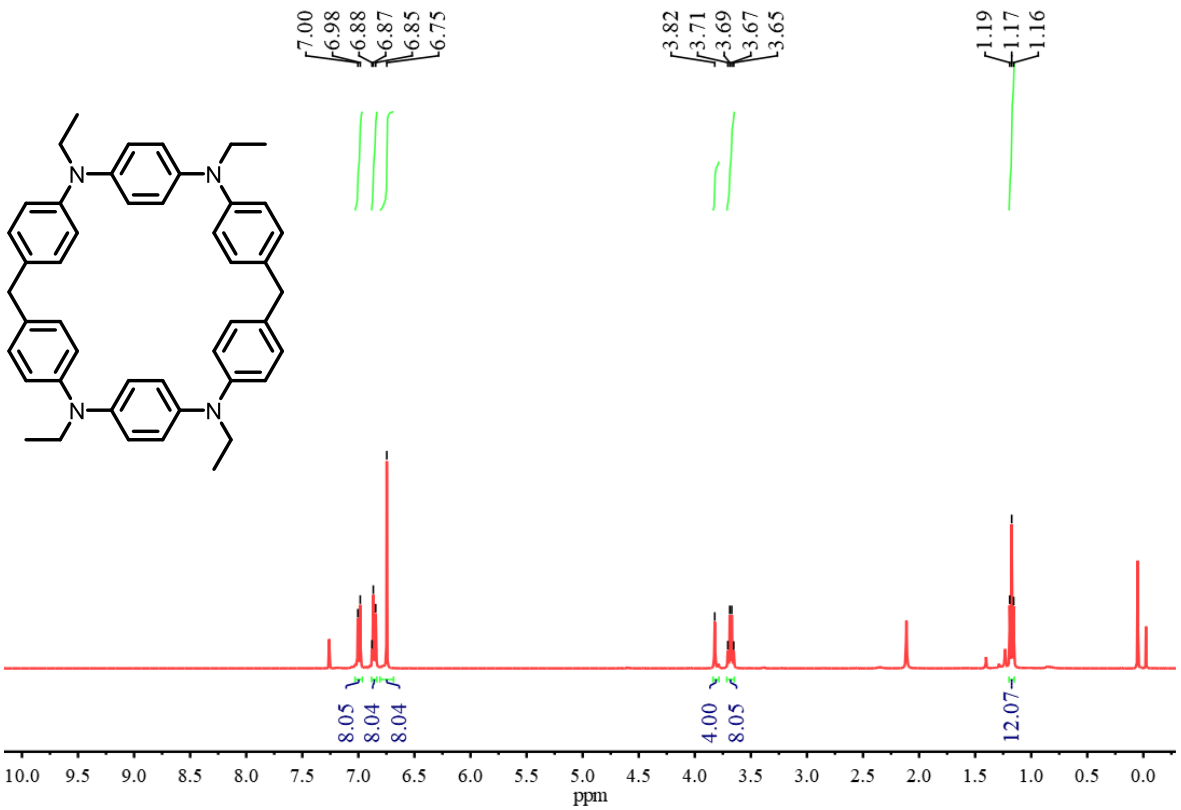

Fig. S9. ^{1}H NMR spectrum of **EtAn[2]** measured in $CDCl_3$ at 25 °C.

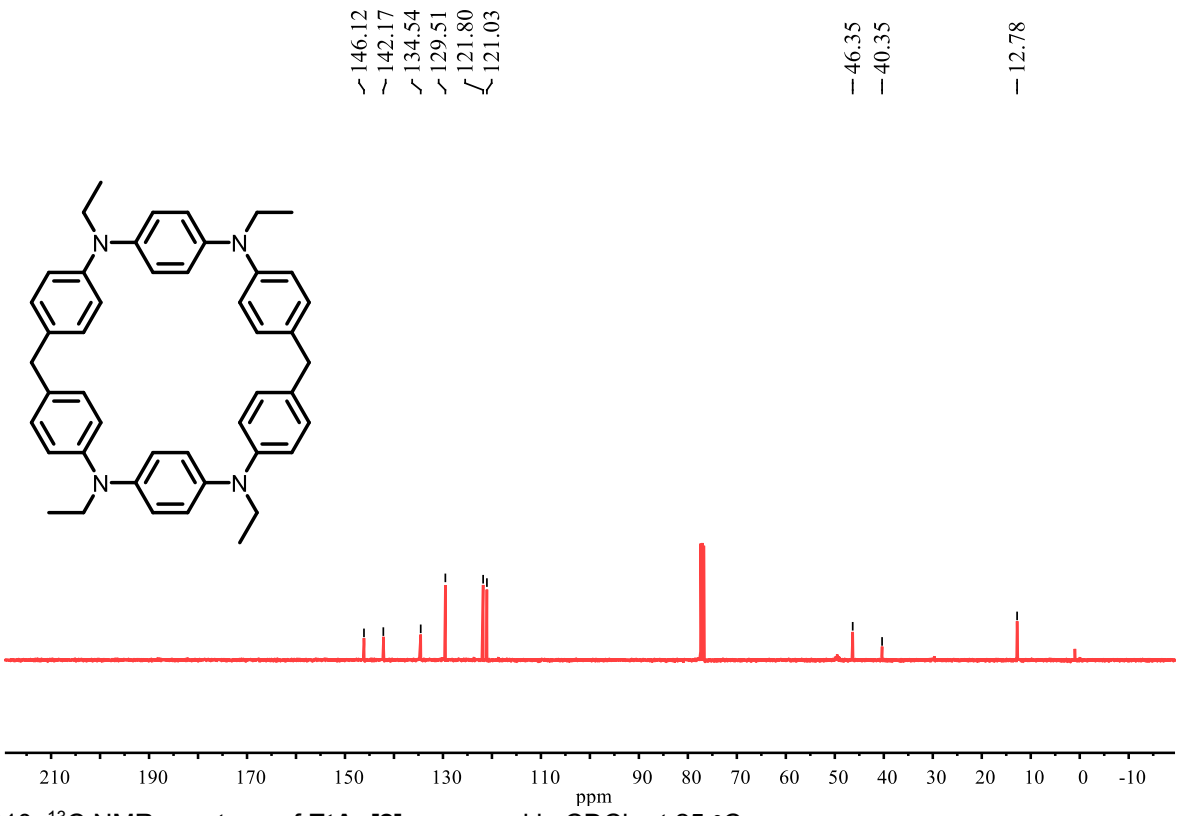

Fig. S10. ^{13}C NMR spectrum of **EtAn[2]** measured in $CDCl_3$ at 25 °C.

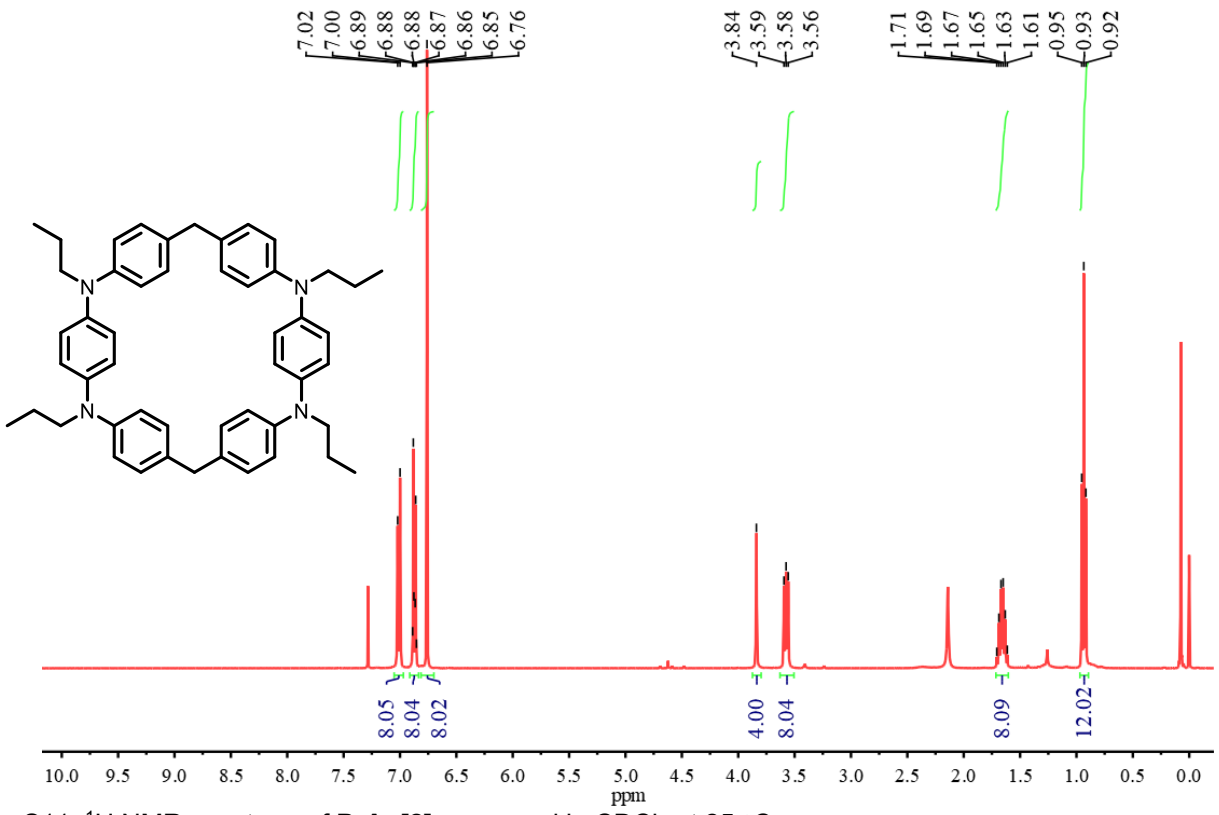

Fig. S11. ^{1}H NMR spectrum of **PrAn[2]** measured in $CDCl_3$ at 25 °C.

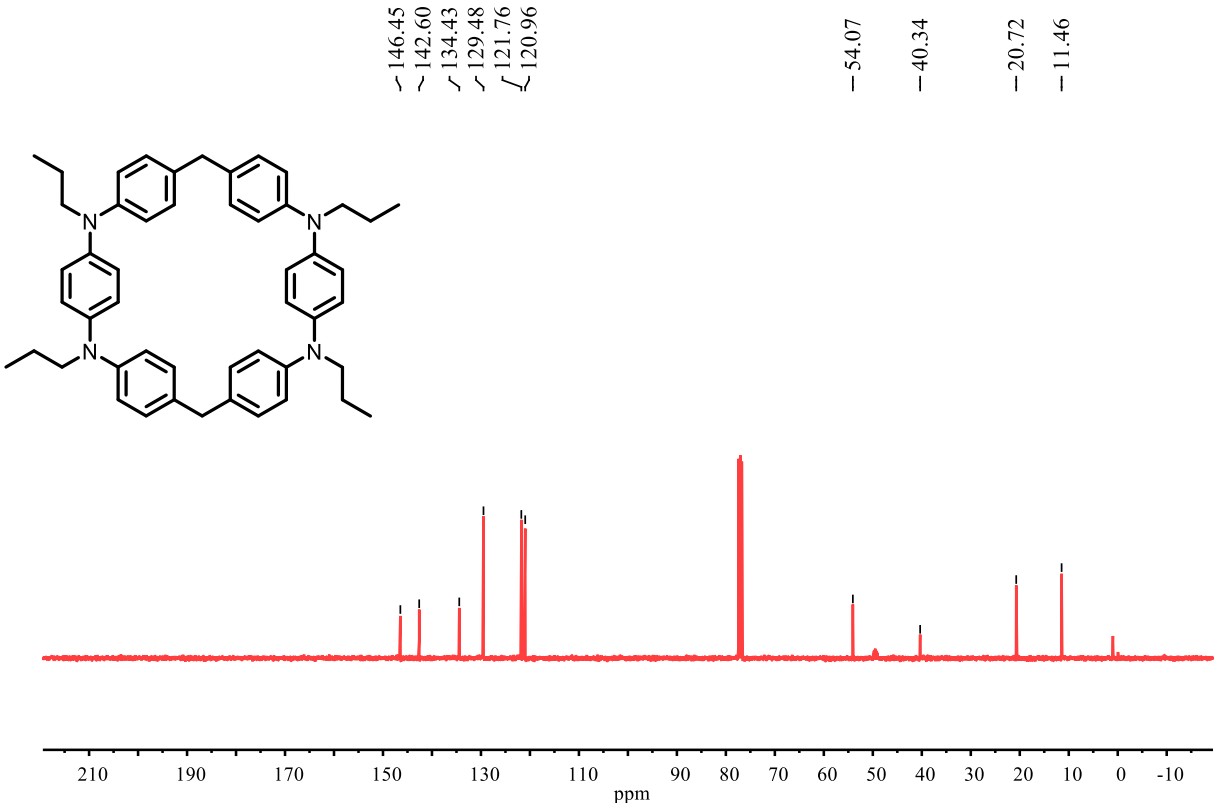

Fig. S12. ^{13}C NMR spectrum of **PrAn[2]** measured in $CDCl_3$ at 25 °C.

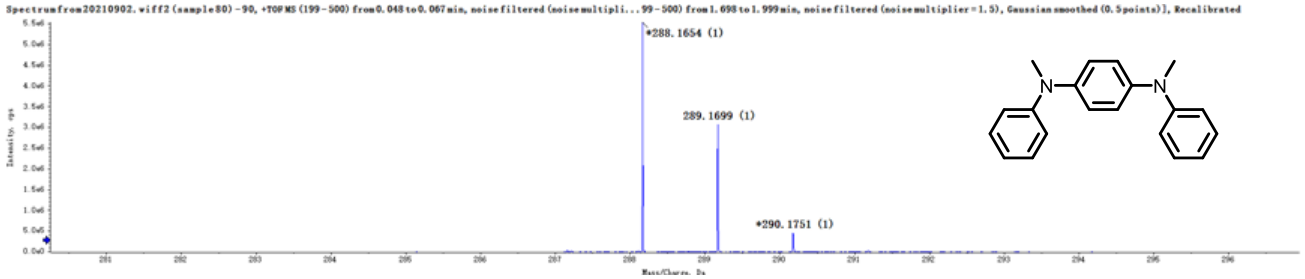

Fig. S13. HRMS spectrum of **MeAn.**

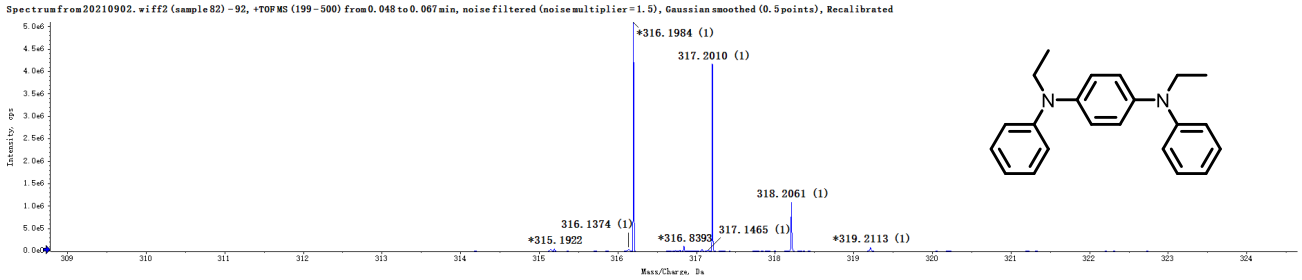

Fig. S14. HRMS spectrum of **EtAn.**

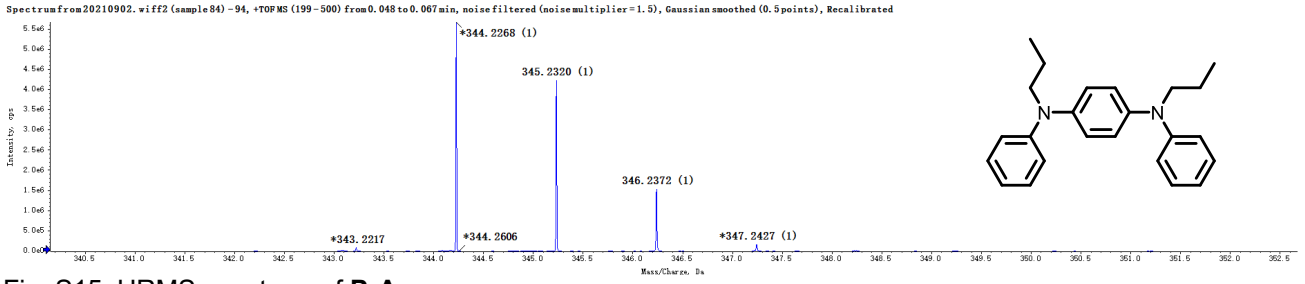

Fig. S15. HRMS spectrum of **PrAn.**

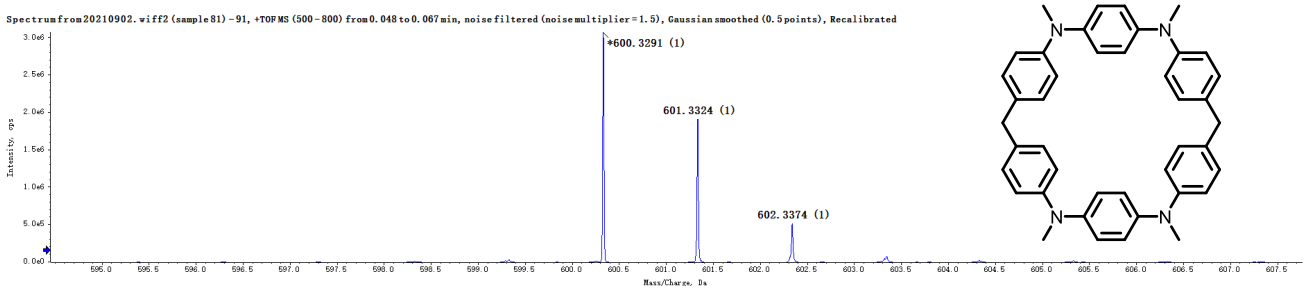

Fig. S16. HRMS spectrum of **MeAn[2].**

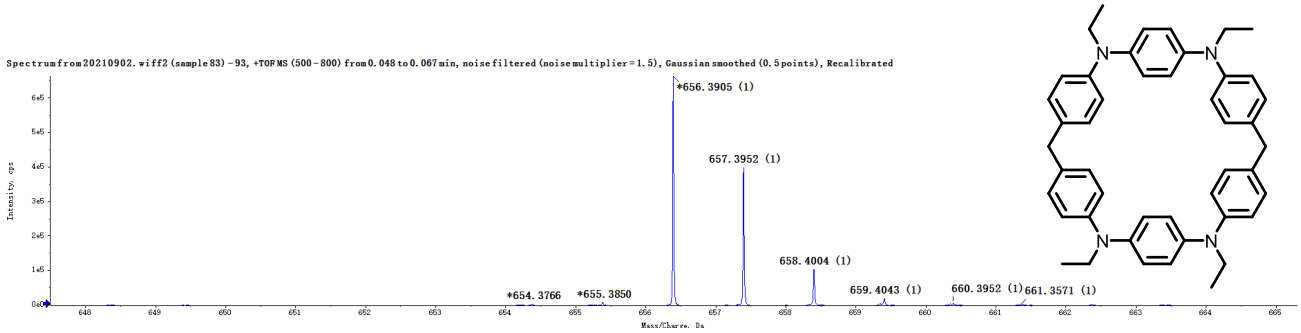

Fig. S17. HRMS spectrum of **EtAn[2].**

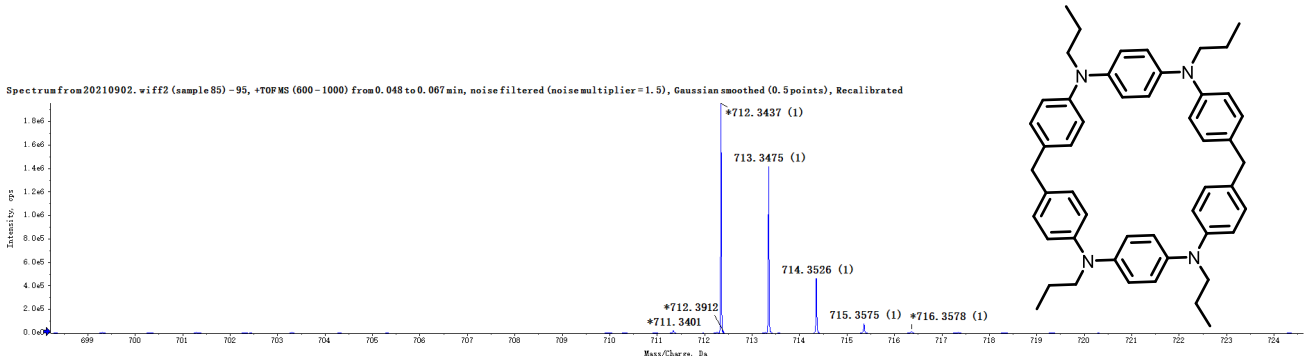

Fig. S18. HRMS spectrum of **PrAn[2].**

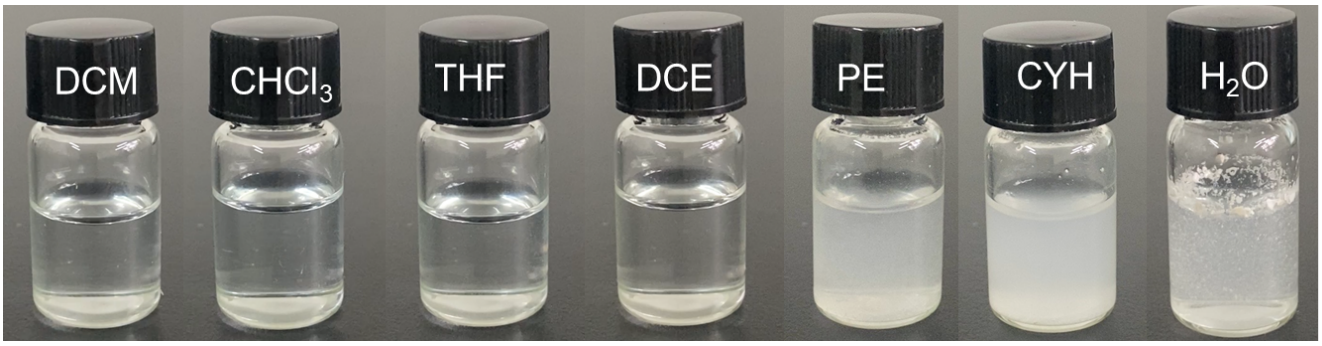

Fig. S19. Solubility testing of EtAn[2] in various organic solvents and water, where 5 mg of EtAn[2] was put into 2 mL dichloromethane(DCM), chloroform($CHCl_3$), tetrahydrofuran(THF), 1,2-dichloroethane(DCE), petroleum ether(PE), cyclohexane(CYH) and water, respectively, and was sonicated for 30 min at room temperature.

N_2 adsorption/desorption isotherms of P-Ns

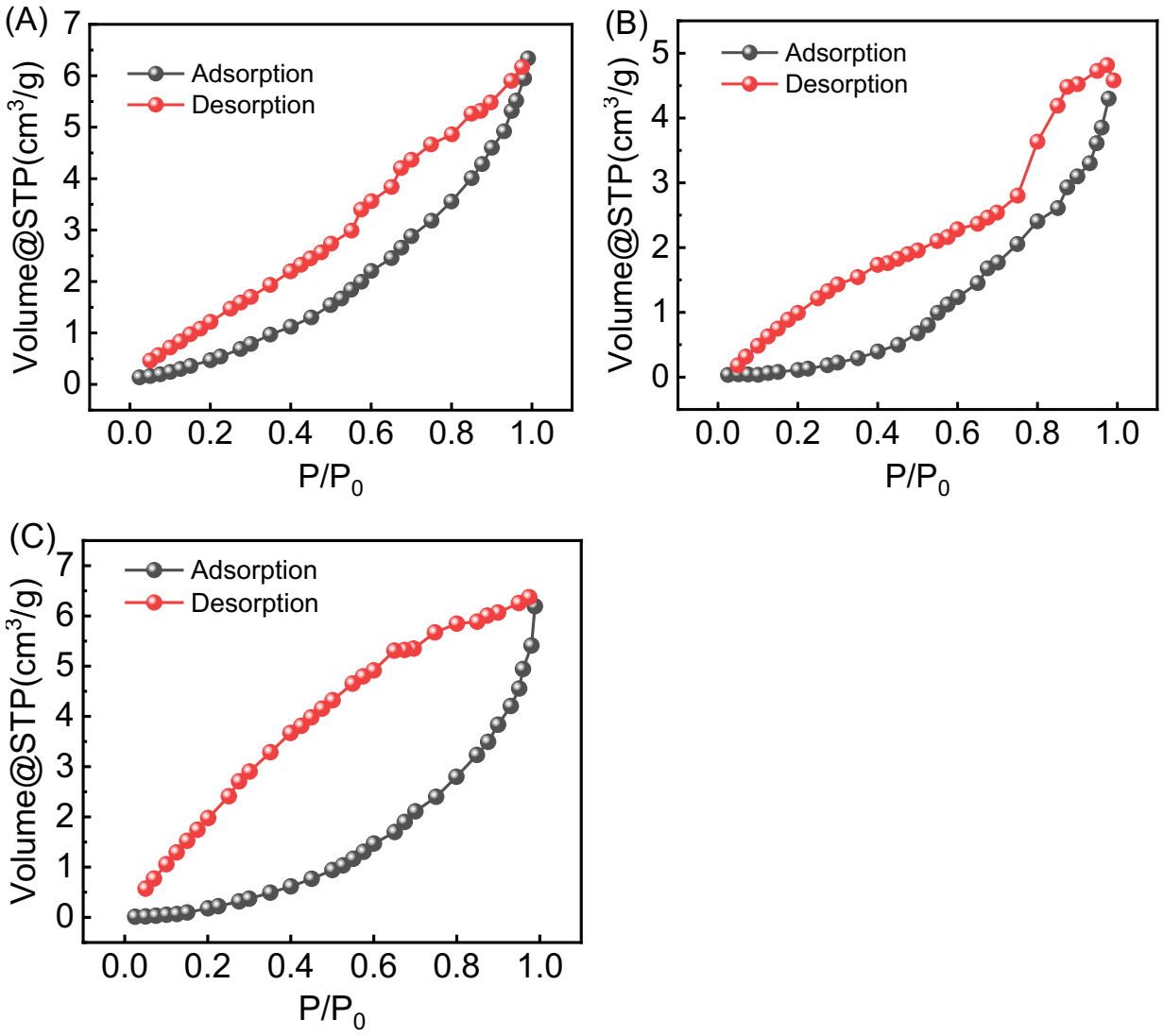

Fig. S20. N_2 adsorption/desorption isotherm of (A) **P-A**, (B) **P-B** and (C)**P-C**.

Table S2. Porosity parameters of the **An[2]**s in the present study.

	S_{BET} ($m^2\ g^{-1}$)	Pore Volume ($cm^3\ g^{-1}$)	Half Pore Width (nm)
MeAn[2]	10.452	0.010	2.520
EtAn[2]	11.856	0.012	1.876
PrAn[2]	12.569	0.010	1.347
P-A	10.891	0.012	4.737
P-B	10.596	0.010	1.877
P-C	12.156	0.013	5.057

Cyclic voltammograms experiments

In order to study the oxidation reduction potential of the precursors(Ans) and An[2]s, CVs of 1.0 mM solutions of all compounds in MeCN with 0.1 M $TBAPF_6$ electrolyte were measured(scan rate =100 mV s^{-1}) as shown in Fig. S27.In the pseudo-reversible / irreversible electrochemical process, the relationship between the peak potential and the scan rate can be expressed according to the method demonstrated by Laviron's model[3] (1), which can be used to calculate the number of electronic transfers. At higher scan rate (0.9 -10 V s^{-1}), a good linear relationship between the logarithm of the scan rate (log v) and the redox potentials was found as shown in Fig. S27.

$$E_{pa} = E^0 + \left(\frac{2.303RT}{\alpha nF}\right)\log\left(\frac{RTk}{\alpha nF}\right) + \left(\frac{2.303RT}{\alpha nF}\right)\log v \quad (1)$$

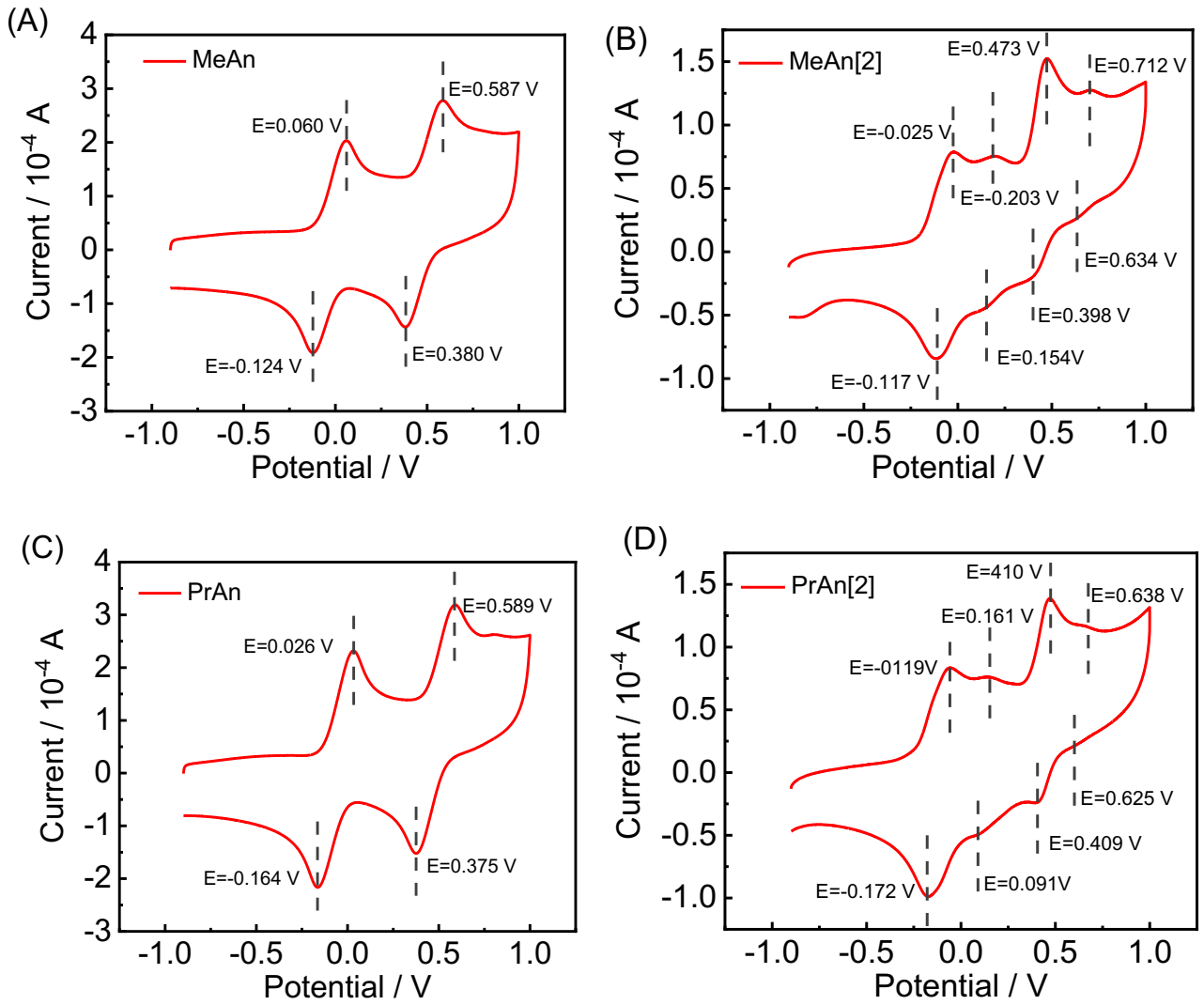

Fig. S21. CVs of 1.0 mM solutions of (A)**MeAn**, (B)**MeAn[2]**, (C) **PrAn** and (D) **PrAn[2]** in MeCN with 0.1 M $TBAPF_6$ electrolyte.

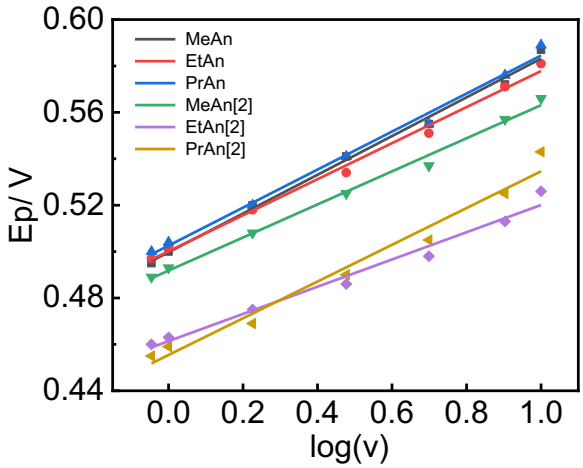

	regression equation	n
MeAn	y=0.0834x+3.8618 R^2=0.9938	1.4174
EtAn	y=0.0777x+6.6418 R^2=0.9933	1.5224
PrAn	y=0.0852x+4.8937 R^2=0.9919	1.4434
MeAn[2]	y=0.0713x+0.4918 R^2=0.9928	1.6590
EtAn[2]	y=0.0587x+0.4614 R^2=0.9768	2.0301
PrAn[2]	y=0.0792x+0.4554 R^2=0.9721	1.4939

Fig. S22. Calibration curve based on the change of the logarithm of the scan rate (0.1-10 V s^{-1}) versus the peak potential (Ep).

Table S3. Element composition and content in polymers.

	C[%]	N[%]	H[%]	S[%]	O[%]	Total[%]
Sulfanilamide[a]	41.815	16.250	4.650	18.620	-----	81.335
benzoic acid[b]	-----	-----	-----	-----	26.200	26.200
P-A[c]	77.320	8.360	5.833	0.000	0.547	92.06

a, CHNS Mode, and Sulfanilamide is used Sulfanilamide as the reference standard

b, O Mode, and Sulfanilamide is used benzoic acid as the reference standard

c, Taking polymer P-A as an example, the composition and content of its element was determined. The total content of the four elements of C, N, O, and H is about 92%, possibly due to that BF_3 remaining during the sample preparation process.

Field emission scanning electron microscope(FESEM) of An[2]s

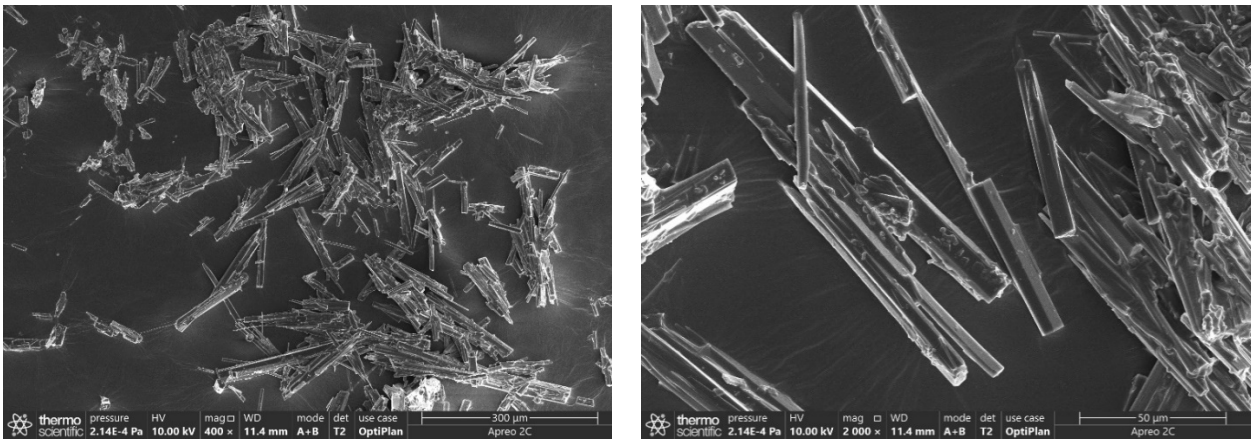

Fig. S23. Scanning electron microscopy images of MeAn[2].

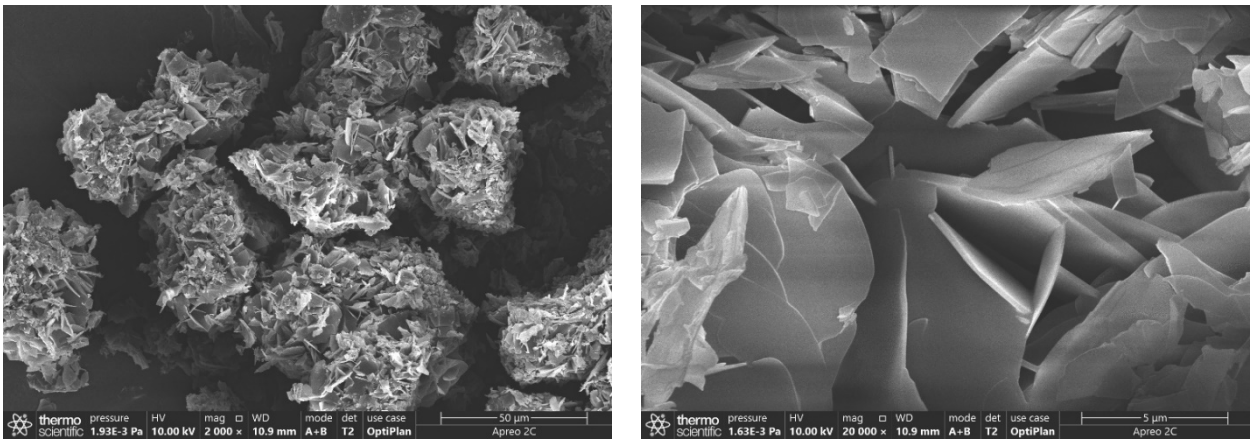

Fig. S24. Scanning electron microscopy images of EtAn[2].

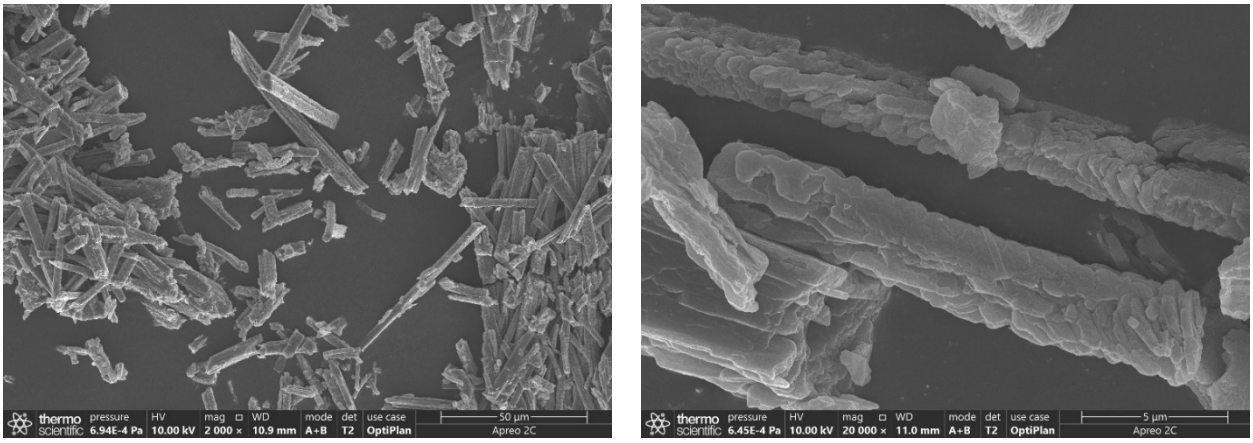

Fig. S25. Scanning electron microscopy images of PrAn[2].

FT-IR spectra of An[2]s and their polymers

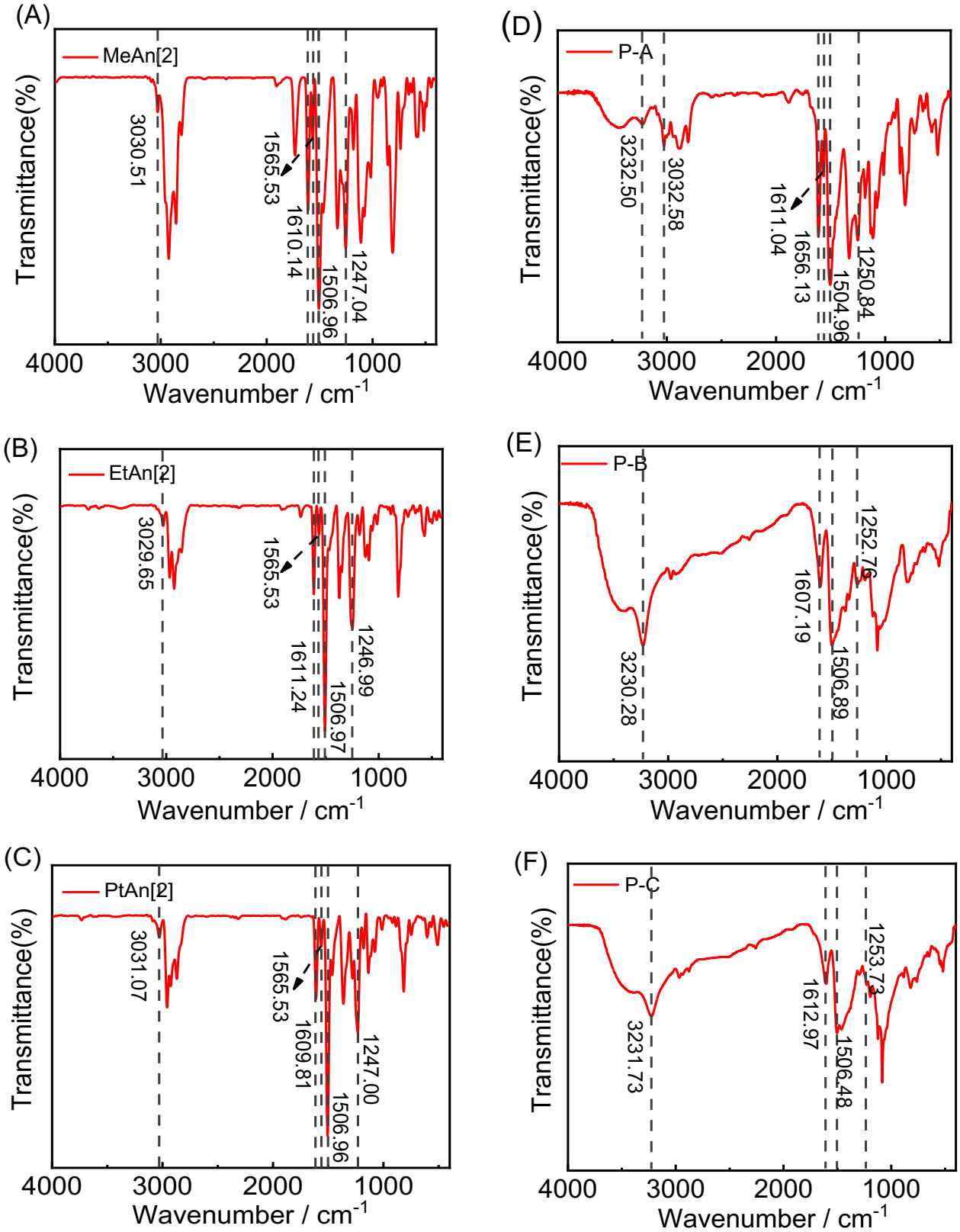

Fig. S26. FT-IR spectra of (A) **MeAn[2]** (B) **Et An[2]**, (C) **Pr An[2]**, (D) **P-A**, (E) **P-B** and (F) **P-C**.

Powder X-ray diffraction pattern of An[2]s

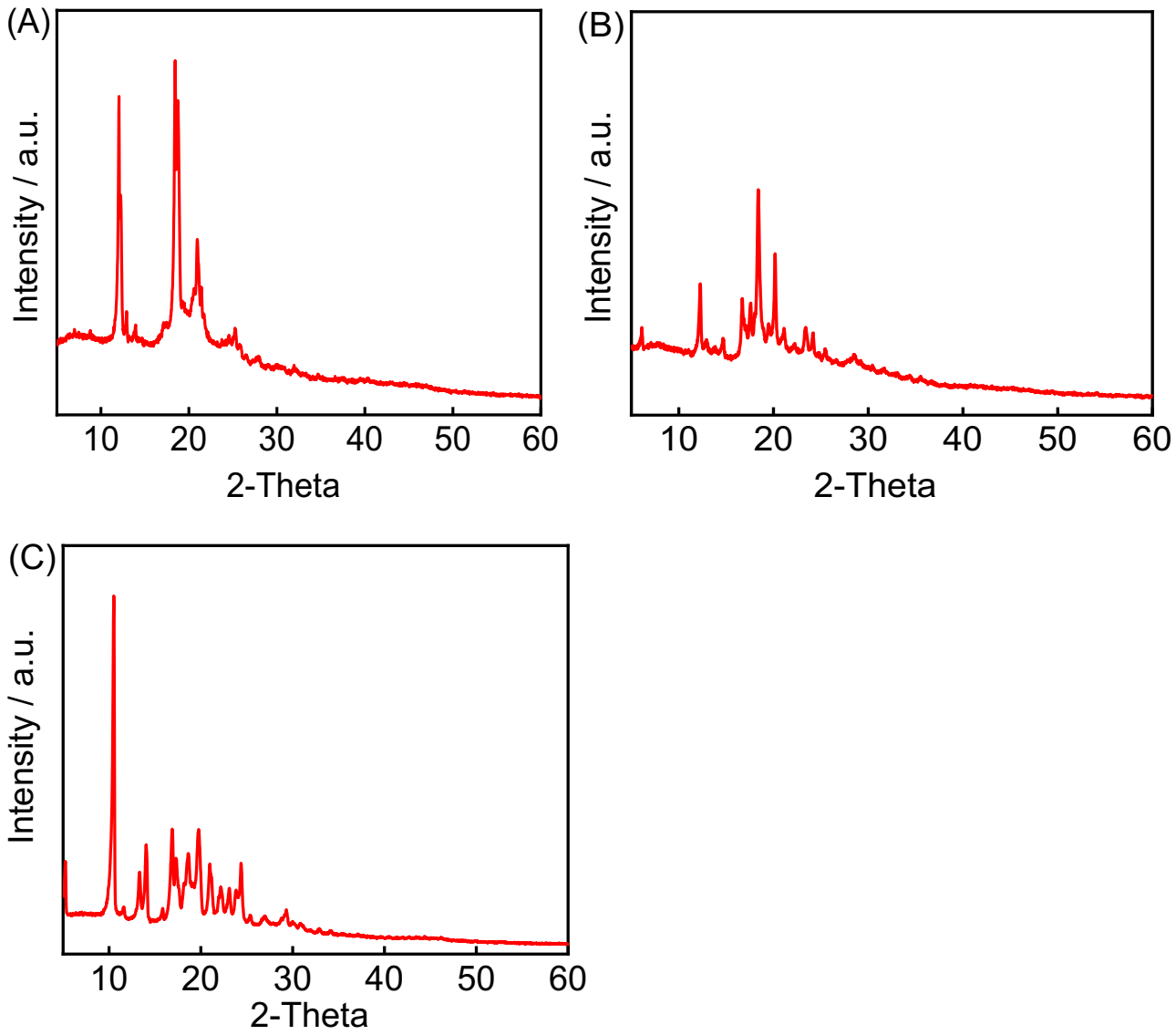

Fig. S27. X-ray powder diffractogram of (A) MeAn[2] , (B) EtAn[2] and (C) PrAn[2].

3. UV-vis and fluorescence spectra of An[2]s

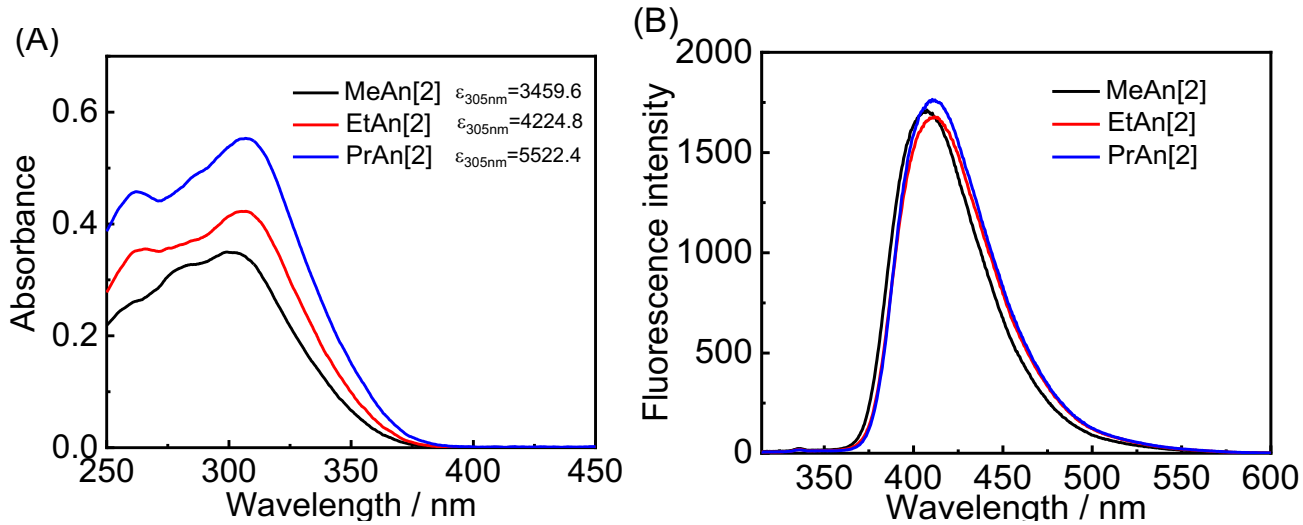

Fig. S28. (A) UV-vis absorption spectra of **MeAn[2]**(100 μM), **EtAn[2]** (100 μM) and **PrAn[2]** (100 μM) in THF at 25 °C. (B) Fluorescence spectra of **MeAn[2]**(10 μM), **EtAn[2]** (10 μM) and **PrAn[2]**(10 μM) in THF at 25 °C, λ_{ex}=305 nm.

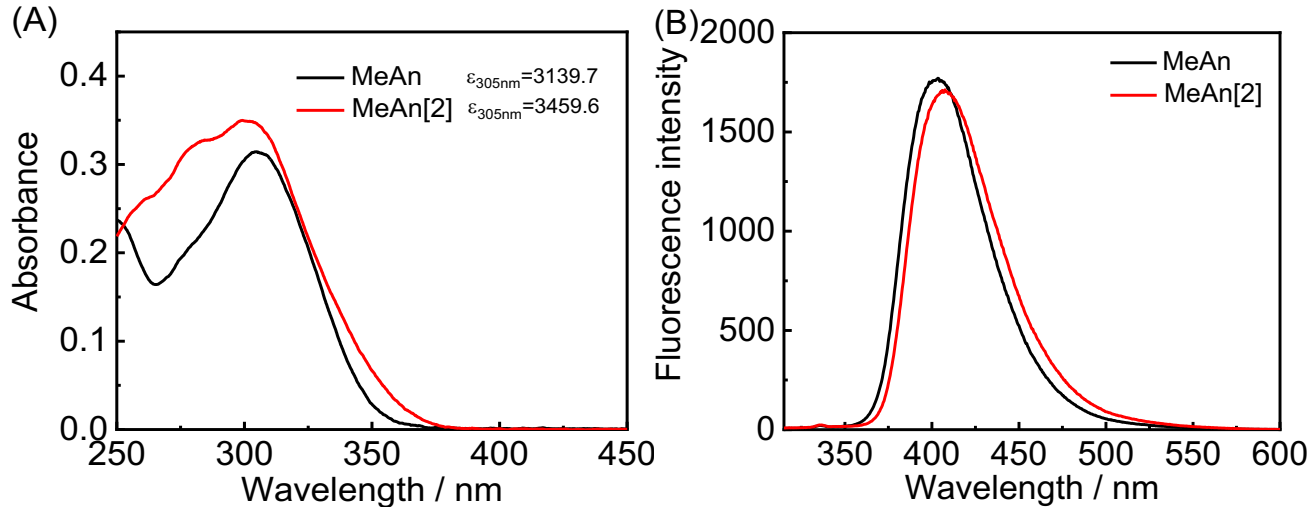

Fig. S29. (A) UV/vis spectra of **MeAn**(100 μM) and **MeAn[2]** (100 μM) in THF at 25 °C, (B) Fluorescence spectra of **MeAn**(10 μM) and **MeAn[2]** (10 μM) in THF at 25 °C, λ_{ex}=305 nm.

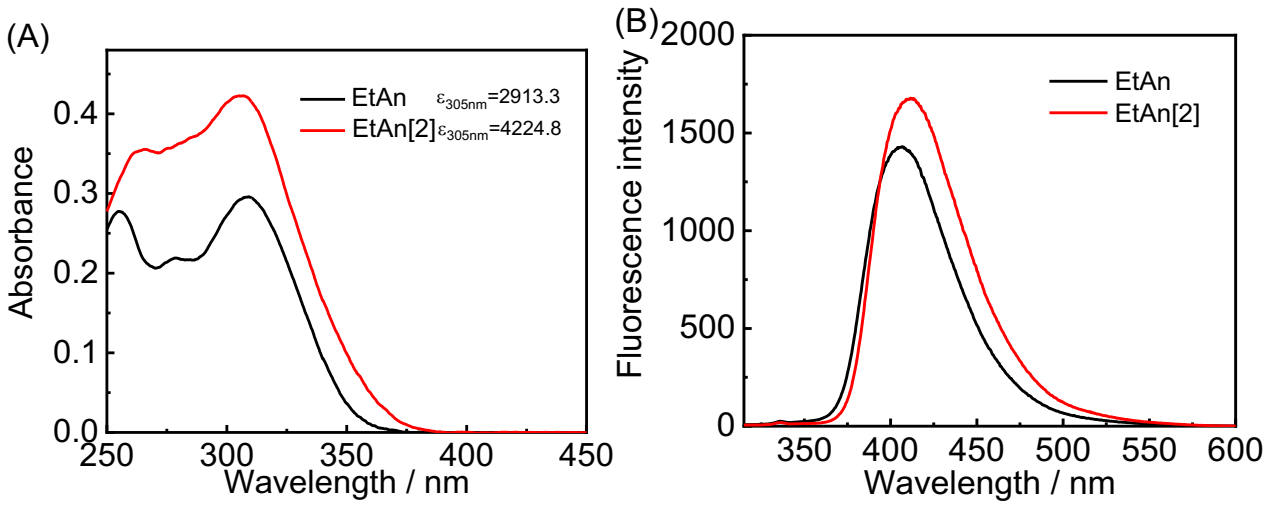

Fig. S30. (A) UV/vis spectra of **EtAn**(100 μM) and **EtAn[2]** (100 μM) in THF at 25 °C, (B) Fluorescence spectra of **EtAn**(10 μM) and **EtAn[2]** (10 μM) in THF at 25 °C, λ_{ex}=305 nm.

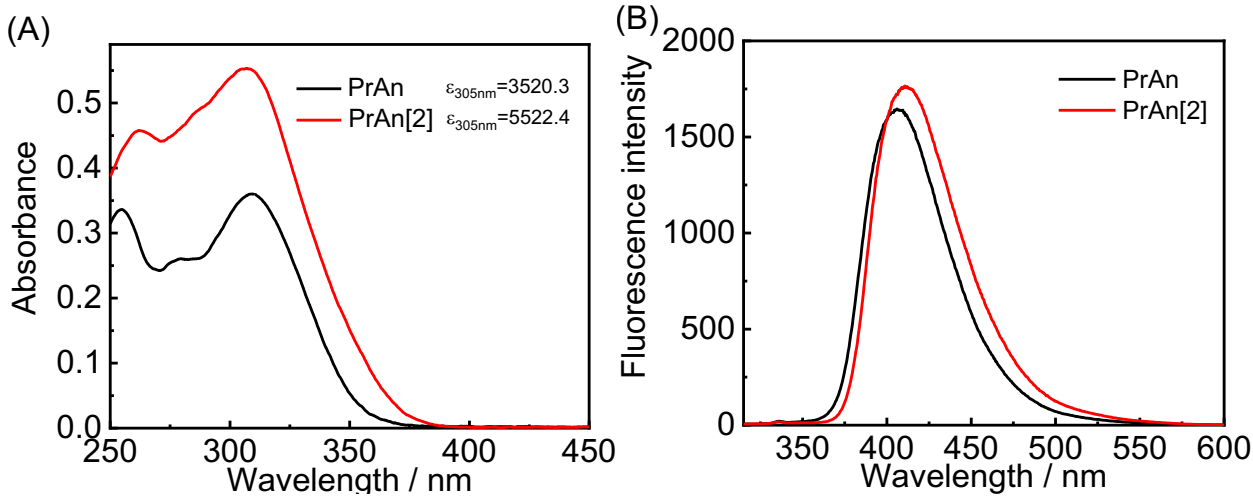

Fig. S31. (A) UV/vis spectra of **PrAn** (100 μM) and **PrAn[2]** (100 μM) in THF at 25 °C, (B) Fluorescence spectra of **PrAn** (10 μM) and **PrAn[2]**(10 μM) in THF at 25 °C, λ_{ex}=305 nm.

4. DFT calculation

Density functional theory (DFT) at B3LYP functional and a 6-31G(d) basis sets were adopted to optimize the structures of the ground state.[1] [2] The optimized structures are shown in Fig. S24.

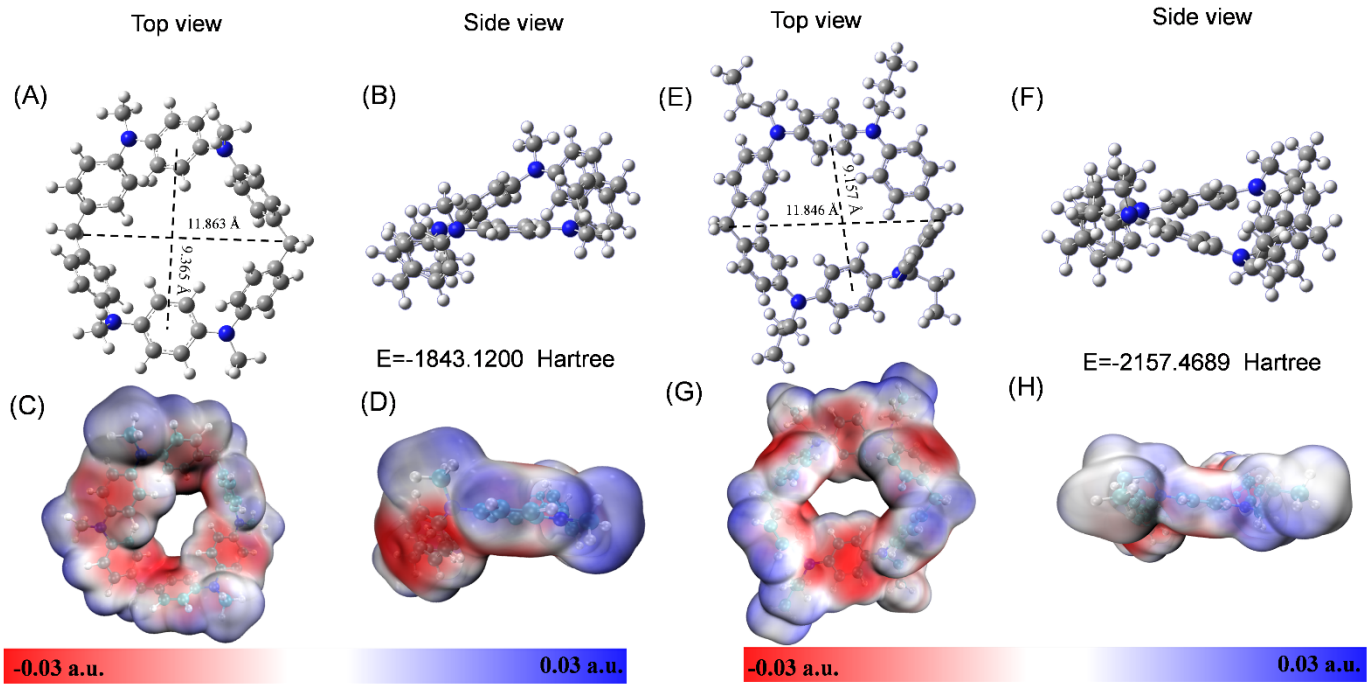

Fig. S32. Optimized structures of (A-D)**MeAn[2]** and (E-H) **PrAn[2]** by DFT at B3LYP/6-31G(d) level. (A and E)Top view and (B and F) Side view of optimized structures of **MeAn[2]** and **PrAn[2]**, respectively. (C and G) Top view and (D and H) Side view of electrostatic potential surface calculated for **MeAn[2]** and **PrAn[2]**, respectively displayed on the isosurface of the electron density at a value of 0.02 e $bohr^{-3}$, with the potential from positively charged regions colored in blue and negatively charged regions colored in red.

5. Iodine vapor capture by An[2]s and P-Ns

The iodine vapor sorption capacities of **An[2]**s were determined by means of gravimetric measurements. The polymer samples were pre-weighed and kept in small weighing vials, which were located in a sealed container with iodine pellets kept at the bottom. The container was degassed and kept at 348.15 K at ambient pressure. The iodine uptake was determined at different time intervals. The values of uptake capacity are the average values of at least two experiments.[4]

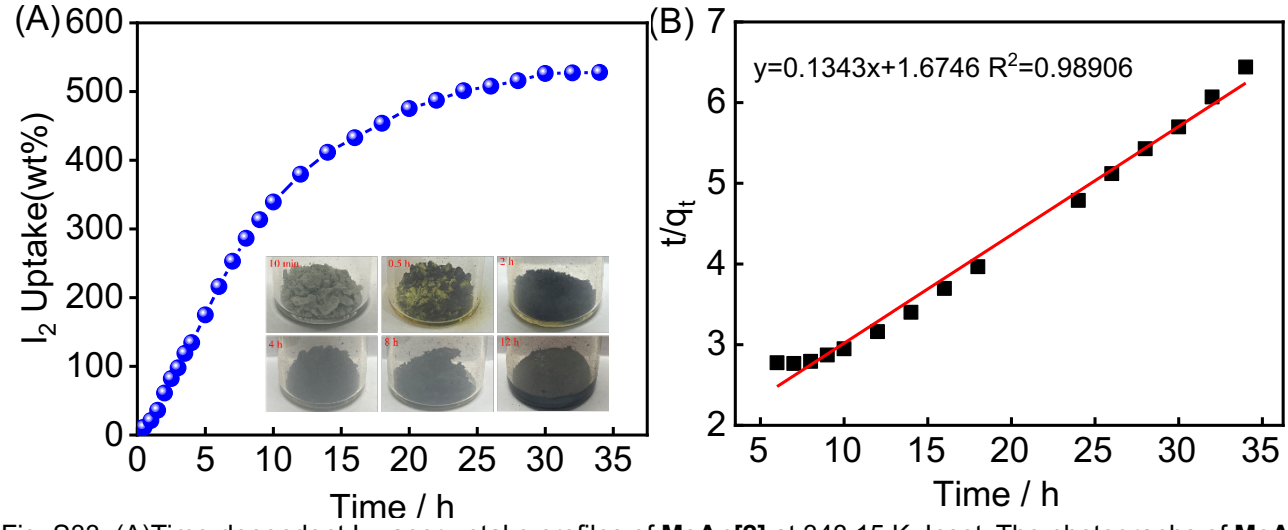

Fig. S33. (A)Time-dependent I_2 vapor uptake profiles of **MeAn[2]** at 348.15 K. Inset: The photographs of **MeAn[2]** upon I_2 vapor uptake at varying time intervals. (B) Line fitting with Pseudo-second-order models for adsorption kinetics data.

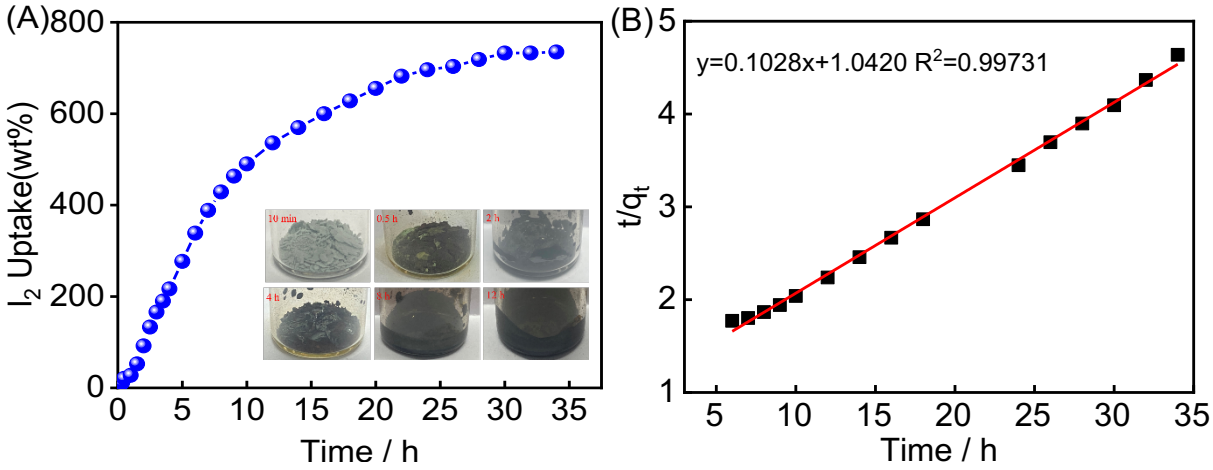

Fig. S34. (A)Time-dependent I_2 vapor uptake profiles of **EtAn[2]** at 348.15 K. Inset: The photographs of **EtAn[2]** upon I_2 vapor uptake at varying time intervals. (B) Line fitting with Pseudo-second-order models for adsorption kinetics data.

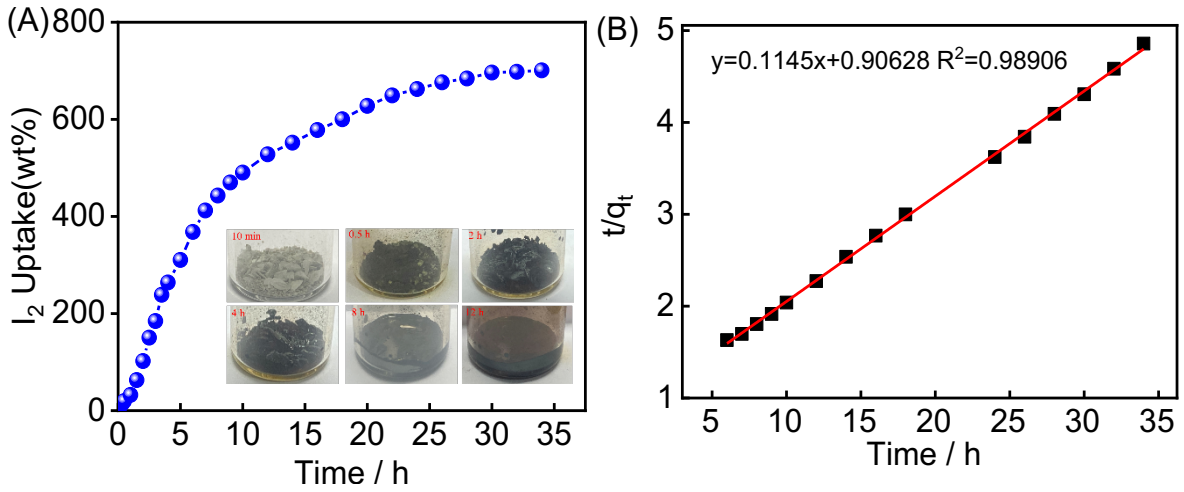

Fig. S35. (A)Time-dependent I_2 vapor uptake profiles of PrAn[2] at 348.15 K. Inset: The photographs of **MeAn[2]** upon I_2 vapor uptake at varying time intervals. (B) Line fitting with Pseudo-second-order models for adsorption kinetics data.

Table S4. Kinetic data corresponding to the iodine vapor adsorption by various **An[2]s** and ACs.

Entry	Slope	Intercept	qe	k_{obs}	R^2
				(g g^{-1} min^{-1})	
MeAn[2]	0.1343	1.6746	5.2800	0.0108	0.9891
EtAn[2]	0.1028	1.0420	7.3521	0.0101	0.9973
PrAn[2]	0.1145	0.9890	7.0125	0.0133	0.9993
ACs[5]	0.4549[5]	3.5402[5]	2.1982[5]	0.0585[5]	0.9997[5]

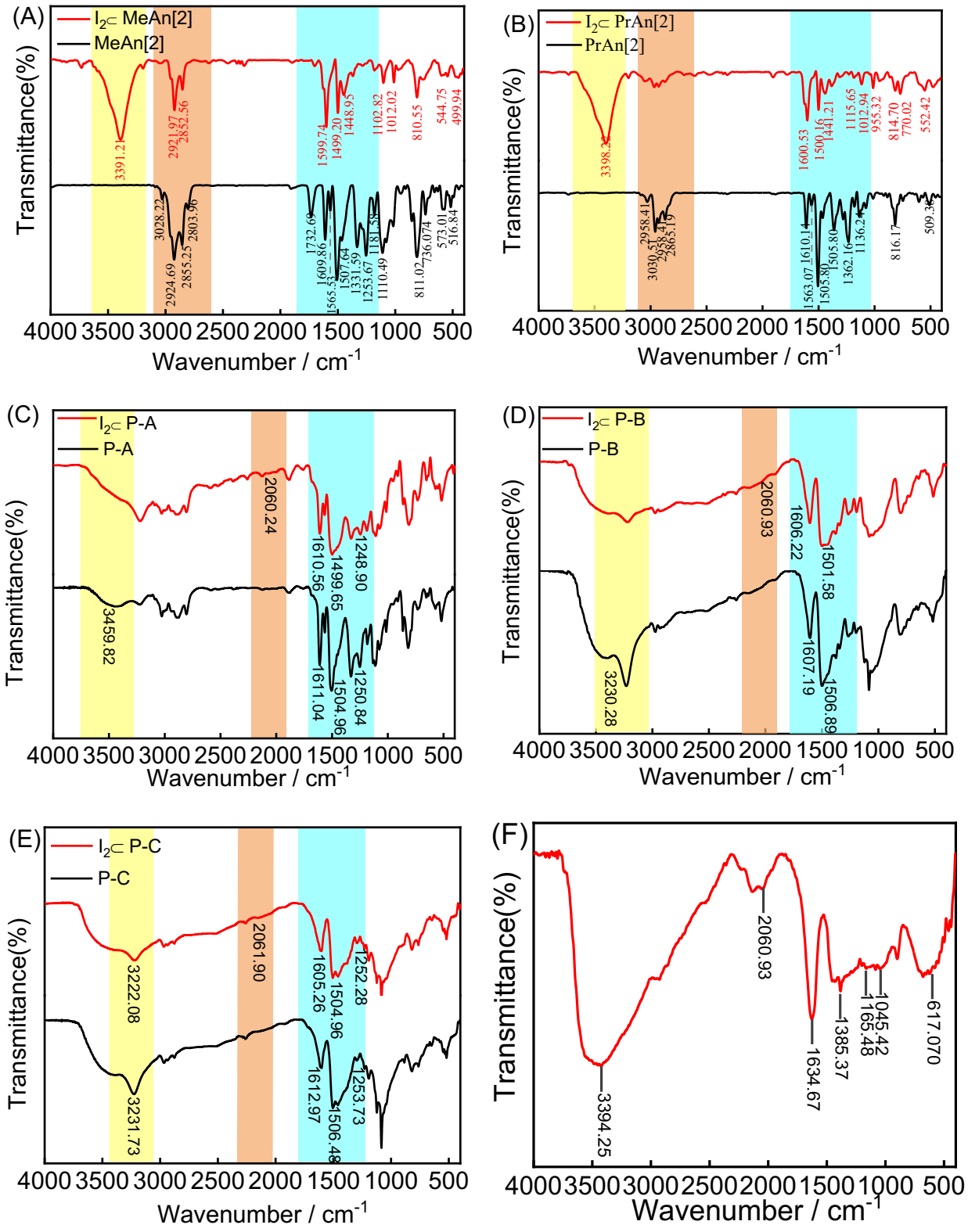

Fig. S36. FT-IR spectra of (A) **MeAn[2]** and I_2⊂**MeAn[2]**, (B) **PrAn[2]** and I_2⊂**PrAn[2]**, (C) **P-A** and I_2⊂ **P-A**, (D) **P-B** and I_2⊂ **P-B**, (E) **P-C** and I_2⊂**P-C**, (F) iodine.

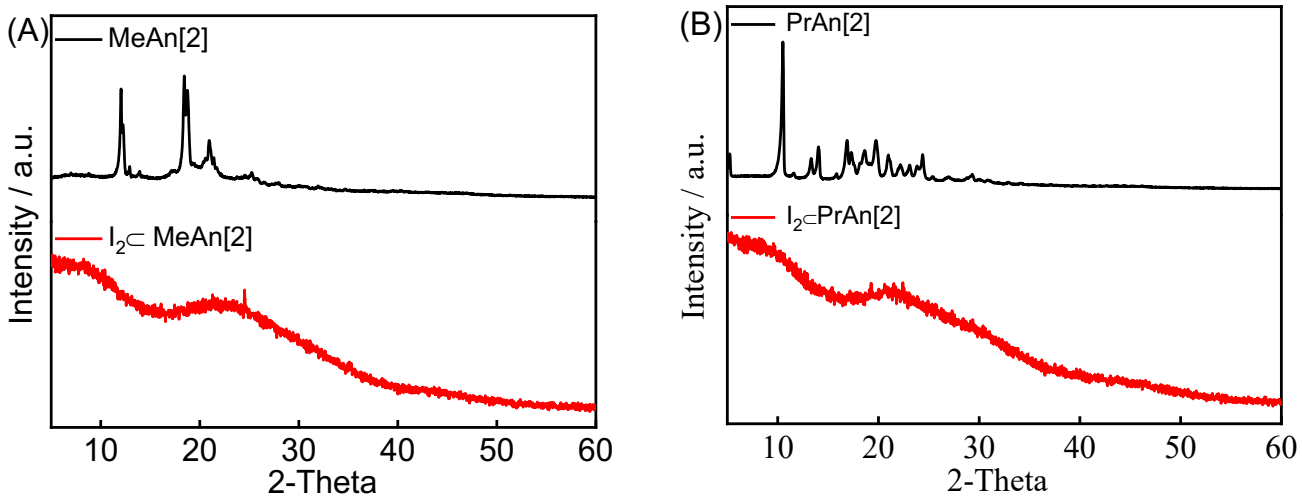

Fig. S37. X-ray powder diffractogram (A) **MeAn[2]** and I_2⊂**MeAn[2]**, (B) **PrAn[2]** and I_2⊂**PrAn[2]**.

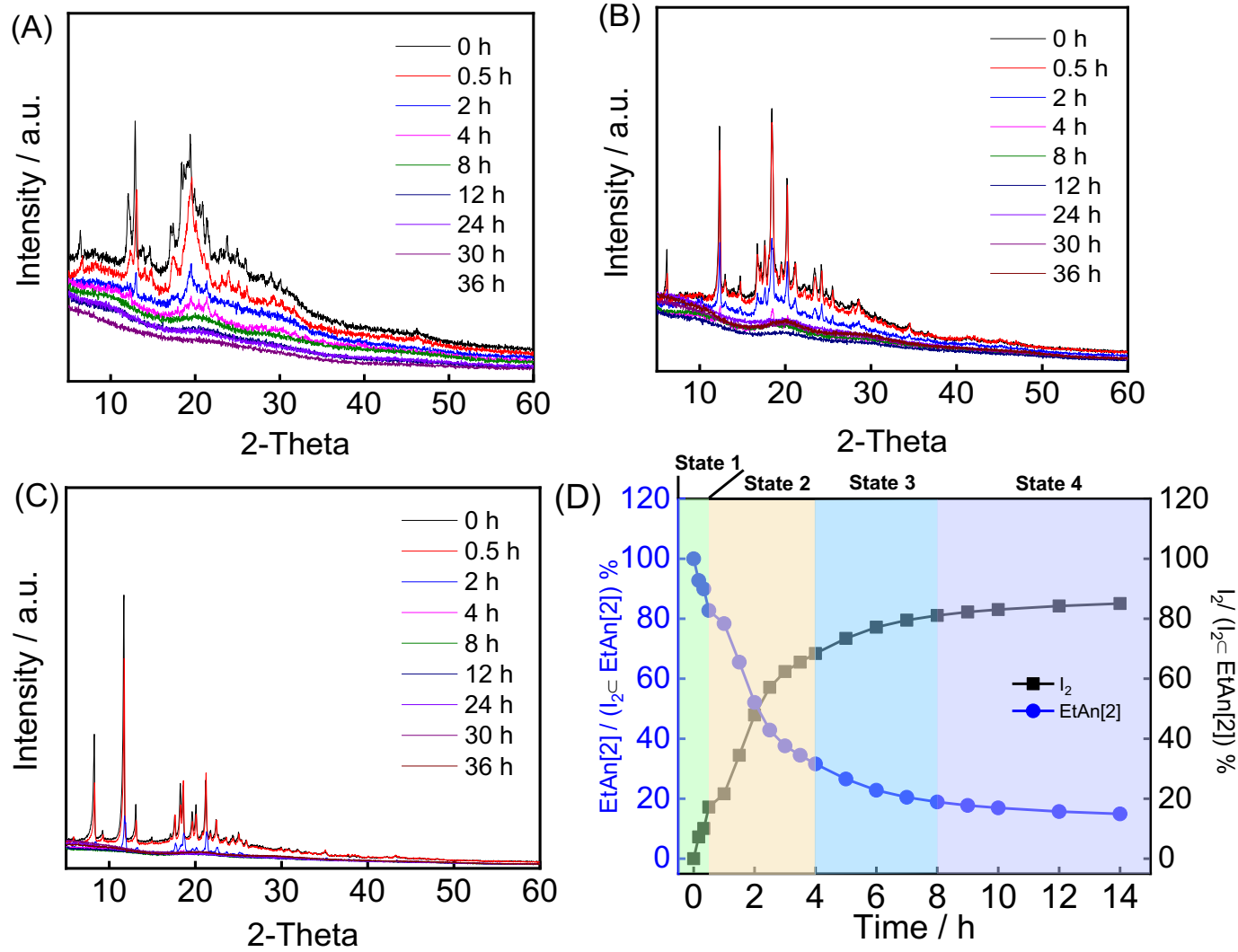

Fig. S38. XRD patterns of (A) **MeAn[2]**, (B) **EtAn[2]**, and (C) **PrAn[2]** after capturing iodine at different time.(D) The process of adsorption of iodine vapor by EtAn[2] can be divided into four stages, labeled as stages 1 to 4, which could be assigned to the surface adsorption, diffusion/reverse dissolution, reverse dissolution, and adsorption equilibrium stages, respectively.

Table S5. Iodine vapor adsorption capacities of macrocycles and Aniline-based materials from 2017-2022.

Materials	Iodine uptake capacity (g g^{-1})	Type	vapor adsorption conditions	Reference
EtAn[2]	7.35	Anilino macrocycle	75 ℃ 30 h	This work
PrAn[2]	7.01	Anilino macrocycle	75 ℃ 30 h	This work
BPPOC	5.64	Porous Organic Cage	75 ℃ 30 h	J. Am. Chem. Soc. 2022, 144, 12390−12399
MeAn[2]	5.28	Anilino macrocycle	75 ℃ 30 h	This work
MeBID[3]	5.12	Bisindole [3]arenes	75 °C 20 h	CCS Chem 2021,3, 1945–1953
P-A	4.91	Aniline-based polymer	75 ℃ 45 h	This work
TTPPA	4.90	Aniline-based polymer	76.85 °C 35 h	*J. Mater. Chem. A*, 2018,6, 2808-2816
CalPOF-1	4.77	Calix[4]resorcinarene	75 ℃ 30 h	ACS Sustain. Chem. Eng., 2018, 6, 17402.
TTPB	4.43	Aniline-based polymer	77 °C 40 h	J. Mater. Chem. A, 2017,5, 7612-7617
CMP-LS5	4.40	Aniline-based polymer	*80* ℃ 8 h	*Polym. Chem.*, *2019*,10, 2608-2615
P-B	4.17	Aniline-based polymer	75 ℃ 45 h	This work
P-C	4.01	Aniline-based polymer	75 ℃ 45 h	This work
C[4]P-BTP	3.38	Calix[4]pyrrole	75 °C 4 h	Angew. Chem. 2021, 133, 2–10
BPy-Cage	3.23	Bipyridine Cage	*75 °C 15 h*	*J. Am. Chem. Soc.* 2022, 144, 1, 113–117
TTDAB	3.13	Aniline-based polymer	76.85 °C 35 h	*J. Mater. Chem. A*, 2018,6, 2808-2816
CalP4-Li	3.12	Calix[4]arenes	*75 °C 10 h*	*Chem. Mater*. 2017, 29, 8968.
C[4]P-TTP	2.99	Calix[4]pyrrole	75 °C 4 h	Angew. Chem. 2021, 133, 2–10
AzoPPN	2.90	Porphyrin-phthalocyanine	*75 °C 10 h*	Chem. Eur. J., 2016, 22, 11863.
CalP3-Li	2.48	Calix[4]arenes	*75 °C 10 h*	*Chem. Mater*. 2017, 29, 8968.
CMP-LS6	2.44	Aniline-based polymer	*80* ℃ 8 h	*Polym. Chem., 2019,10, 2608-2615.*
PAN-FPP5	2.2	Pillar[5]arenes	70 °C 24 h	Ind. Eng. Chem. Res. 2020, 59, 3269.
CMP-4	2.08	Pillar[6]arenes	75 °C 20 h	Angew. Chem. Int. Ed., 2021, 60, 8967.
C[4]P-DPP	1.89	Calix[4]pyrrole	75 °C 4 h	Angew. Chem. 2021, 133, 2–10
CalP2-Li	1.08	Calix[4]arenes	*75 °C 10 h*	*Chem. Mater*. 2017, 29, 8968.
G-TP5	0.67	Terphen[n]arenes	75 °C 1 h	Angew.Chem. Int.Ed. 2019, 58,3885 –3889

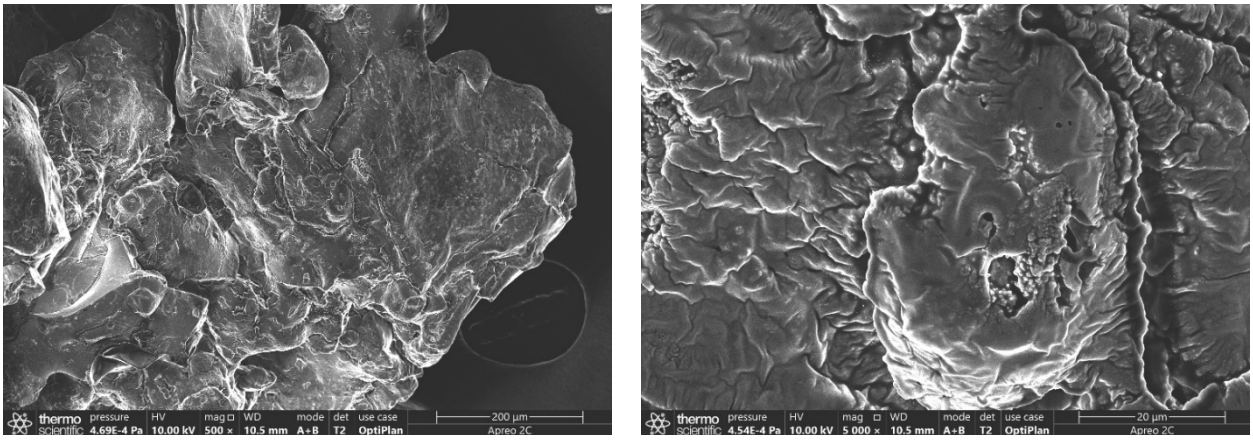

Fig. S39. Scanning electron microscopy images of I_2⊂ **MeAn[2]**.

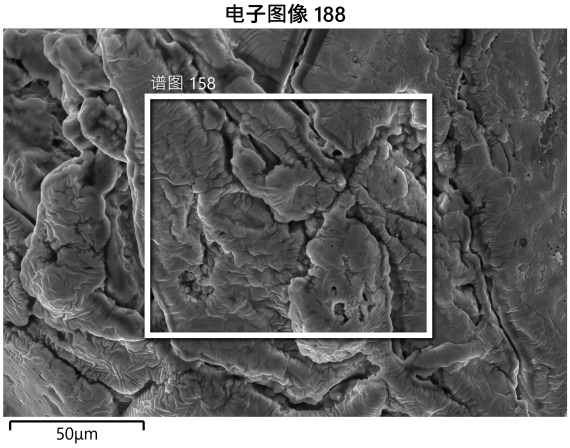

EDS 158		
elements	Wt%	At%
C	32.64	83.58
N	0.05	0.11
I	67.31	16.31
total	100.00	100.00

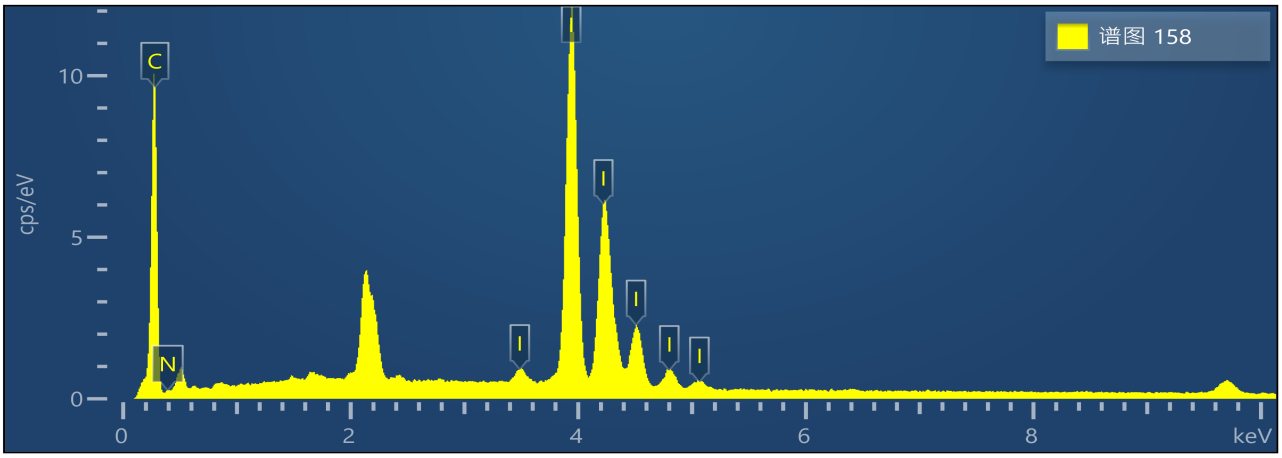

Fig. S40. Energy-dispersive spectroscopy (EDS) analysis profile of I_2⊂ **MeAn[2]**.

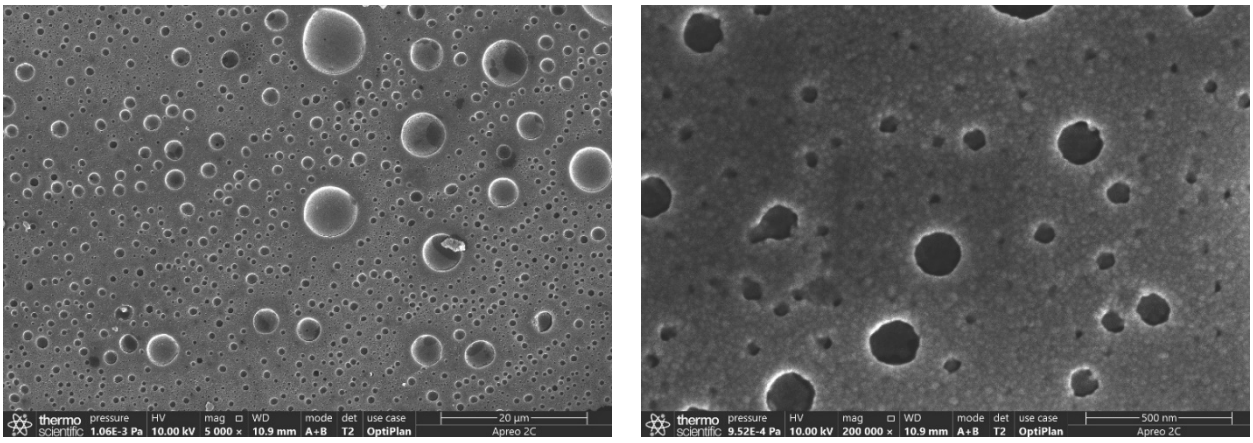

Fig. S41. Scanning electron microscopy images of I_2⊂**EtAn[2]**.

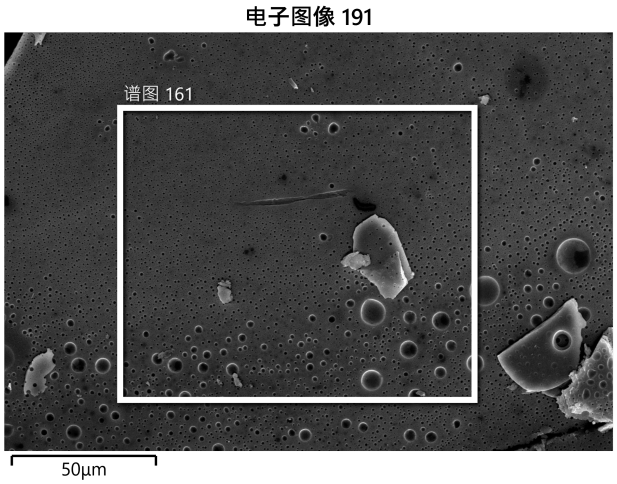

EDS 161		
elements	Wt%	At%
C	27.17	77.25
N	1.45	3.54
I	71.37	19.20
total	100.00	100.00

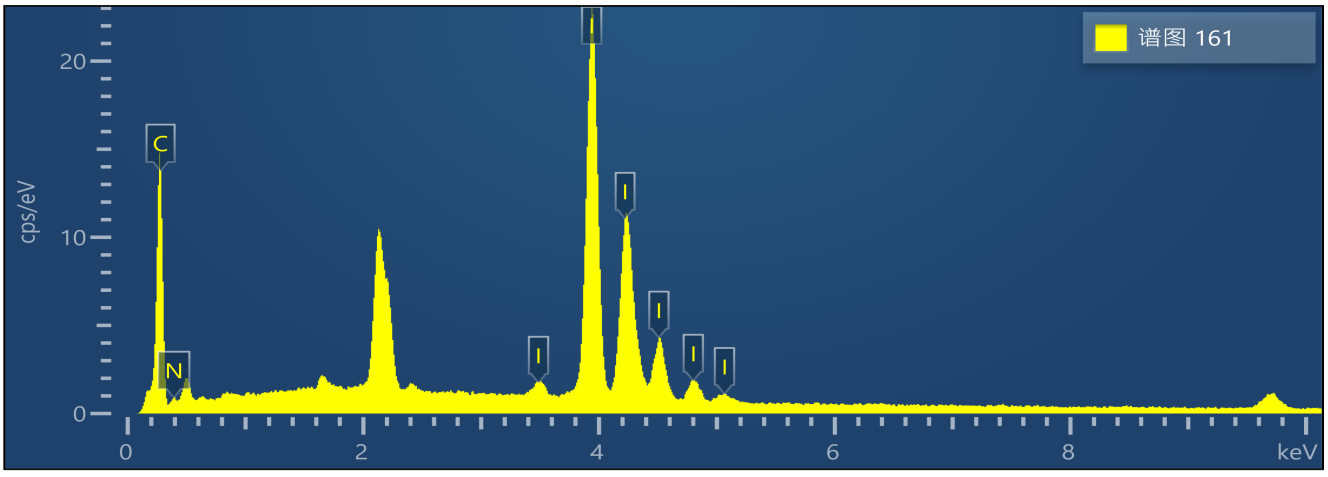

Fig. S42. Energy-dispersive spectroscopy (EDS) analysis profile of I_2⊂**EtAn[2]**.

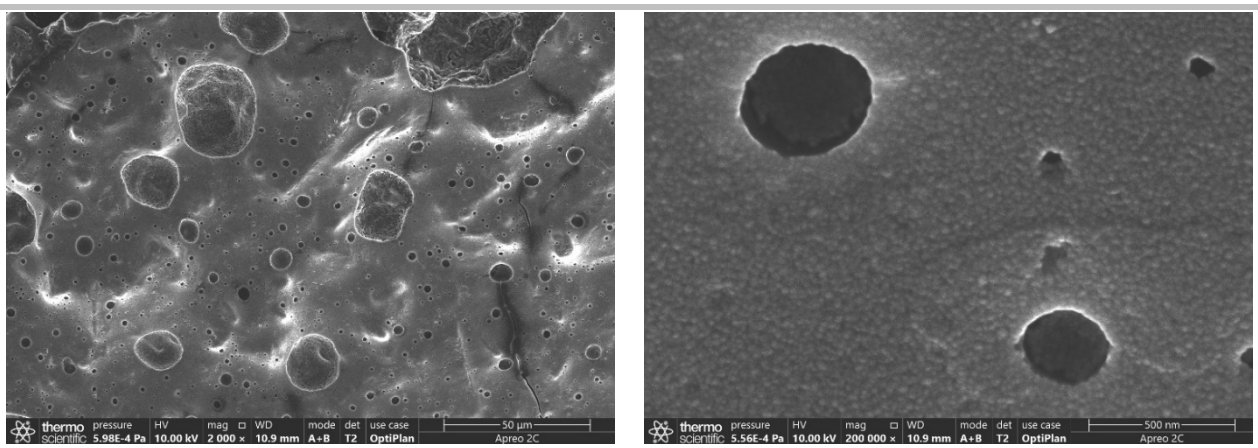

Fig. S43. Scanning electron microscopy images of I_2⊂ PrAn[2].

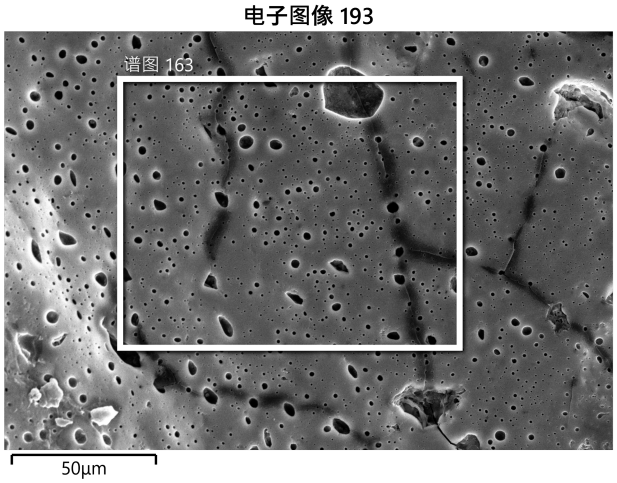

EDS 163		
element	Wt%	At%
C	26.15	76.93
N	1.12	2.82
I	72.73	20.25
total	100.00	100.00

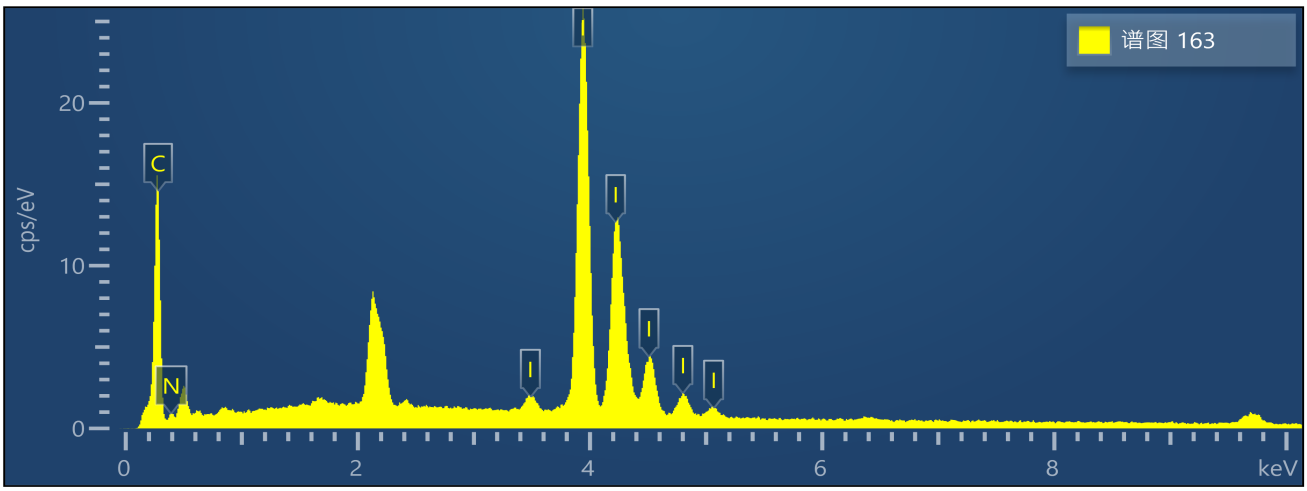

Fig. S44. Energy-dispersive spectroscopy (EDS) analysis profile of I_2⊂ PrAn[2].

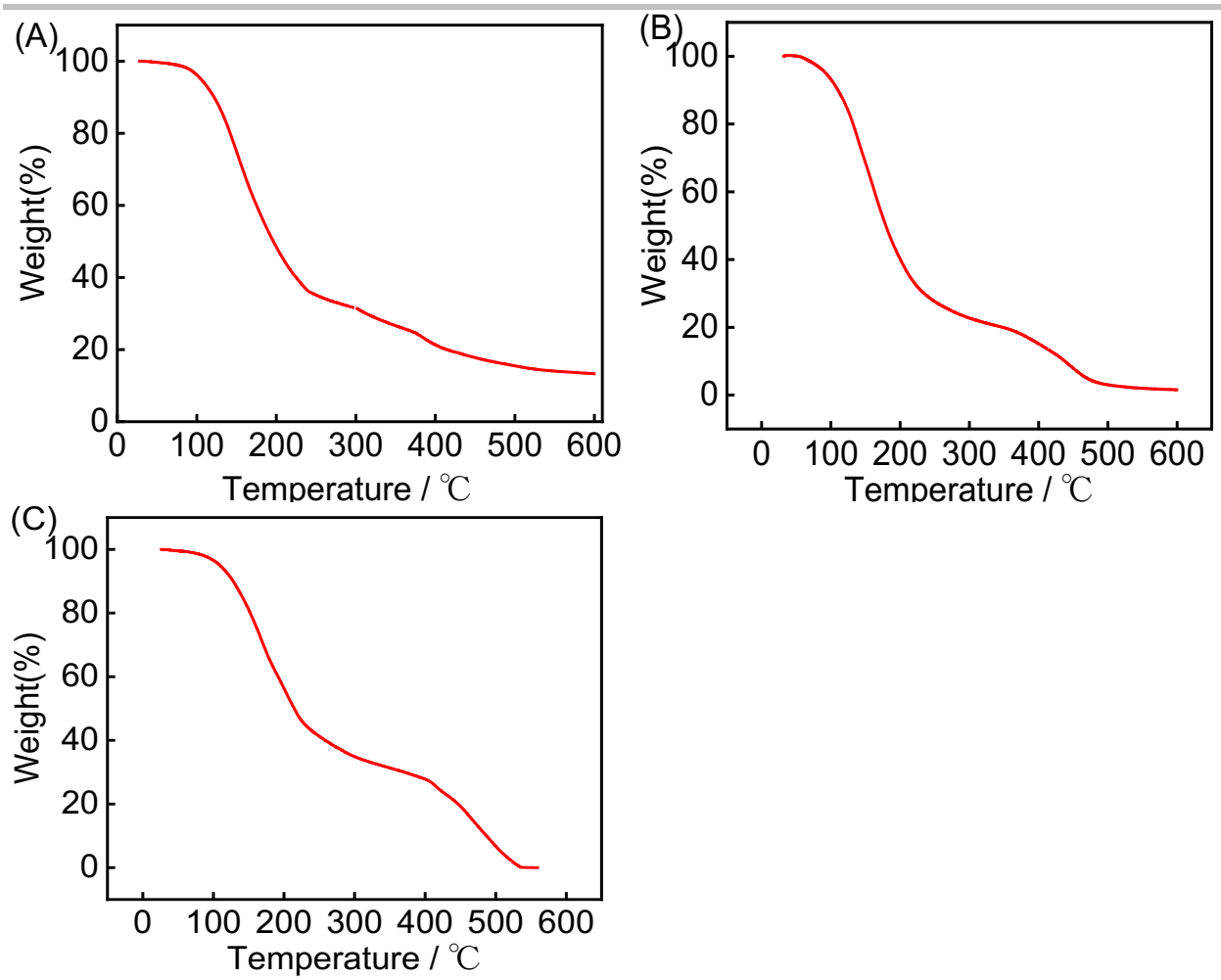

Fig. S45. TGA profiles of (A)I_2⊂ **MeAn[2]**, (B) I_2⊂ **EtAn[2]**, and (C) I_2⊂ **PrAn[2]**.

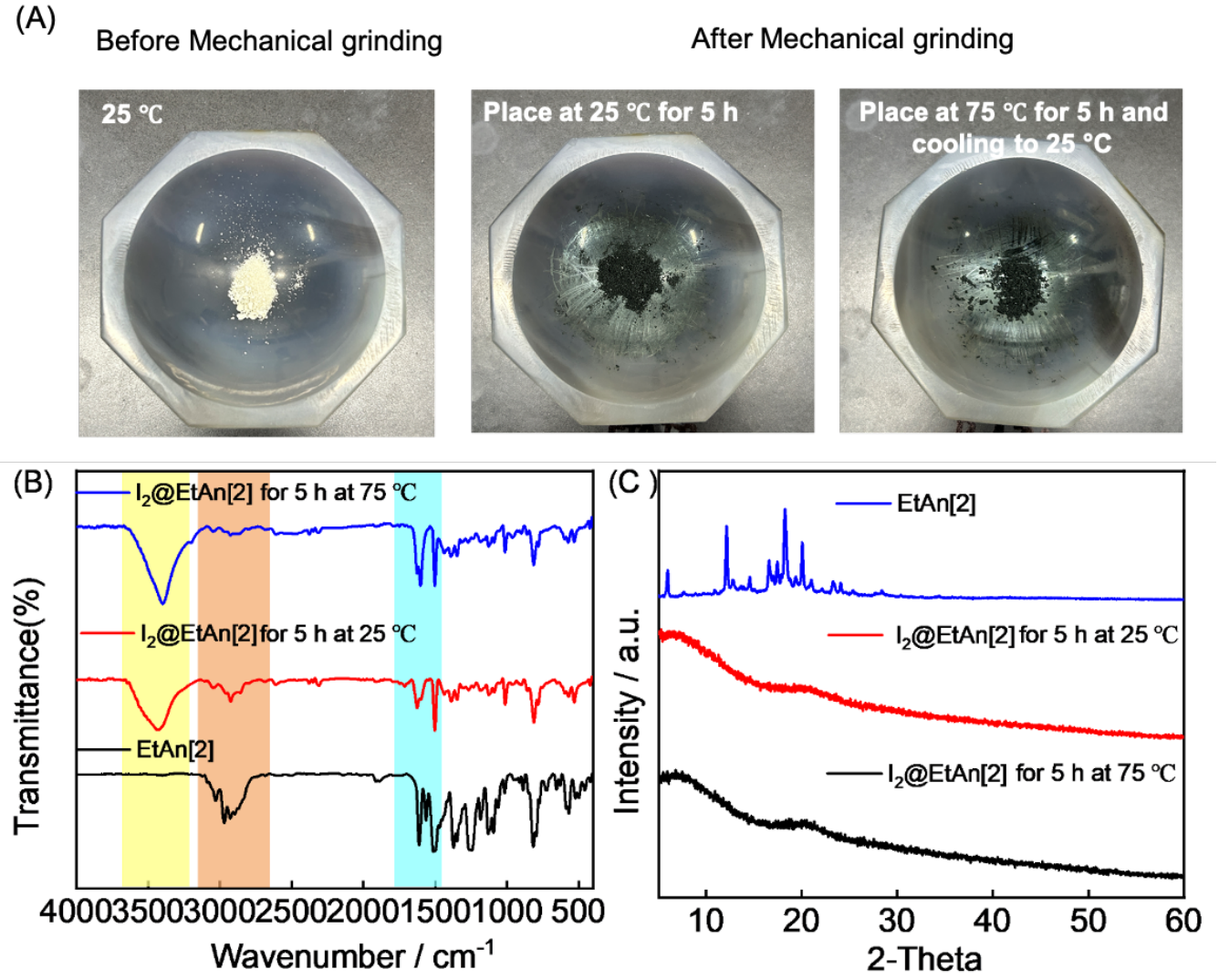

Fig. S46. (A) The photos of iodine and **EtAn[2]** before and after grinding in solid state. The left photo shows that the original state of **EtAn[2]** under 25 ℃; The middle photo shows the state of **EtAn[2]** after grinding and placing for 5 hours at 25 ℃. The right photo shows the state of **EtAn[2]** after grinding at 25 °C, placing at 75 °C for 5 hours and cooling to 25 °C. The mixture of iodine and EtAn[2] after mechanical grinding, the FT-IR(B) and XRD(C) spectrum after 5 hours of placement.

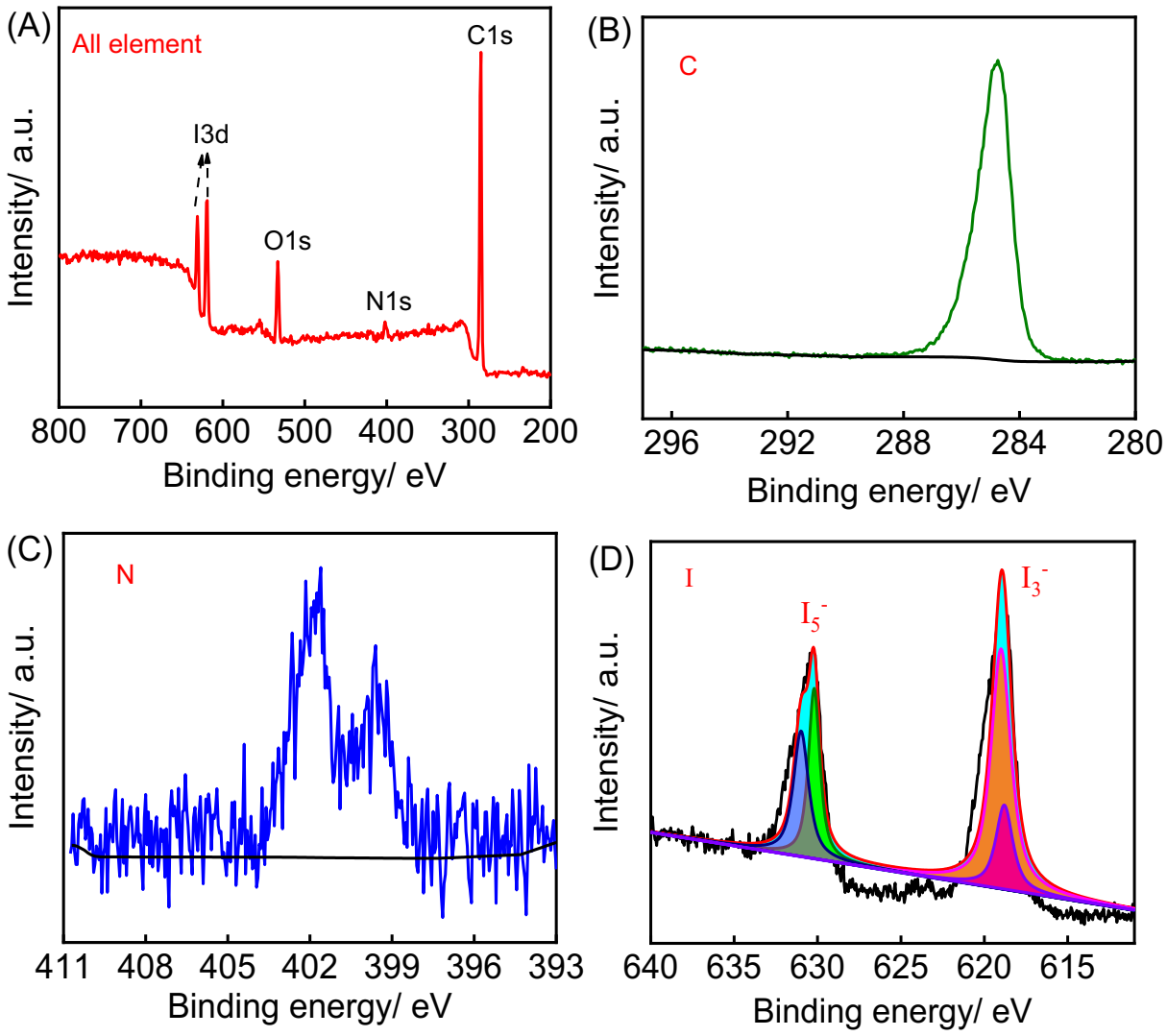

Fig. S47. XPS full spectra of (A) I_2⊂ **MeAn[2]**, (B)C1s, (C) N1s and (D) I3d XPS spectra of I_2⊂ **MeAn[2]**.

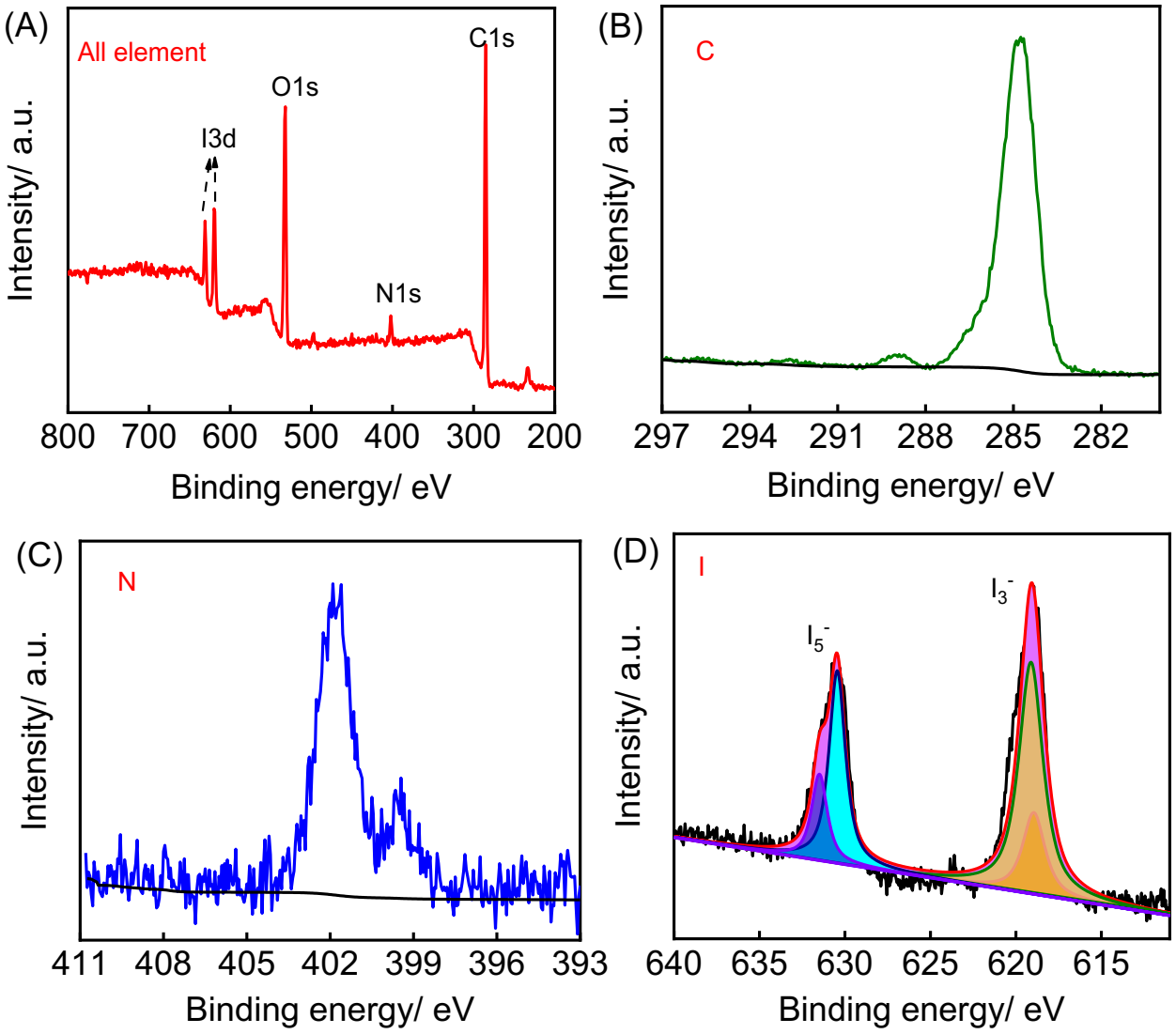

Fig. S48. XPS full spectra of (A)I_2⊂ **EtAn[2]**, (B)C1s, (C)N1s and (D) I3d XPS spectra of I_2⊂ **EtAn[2]**.

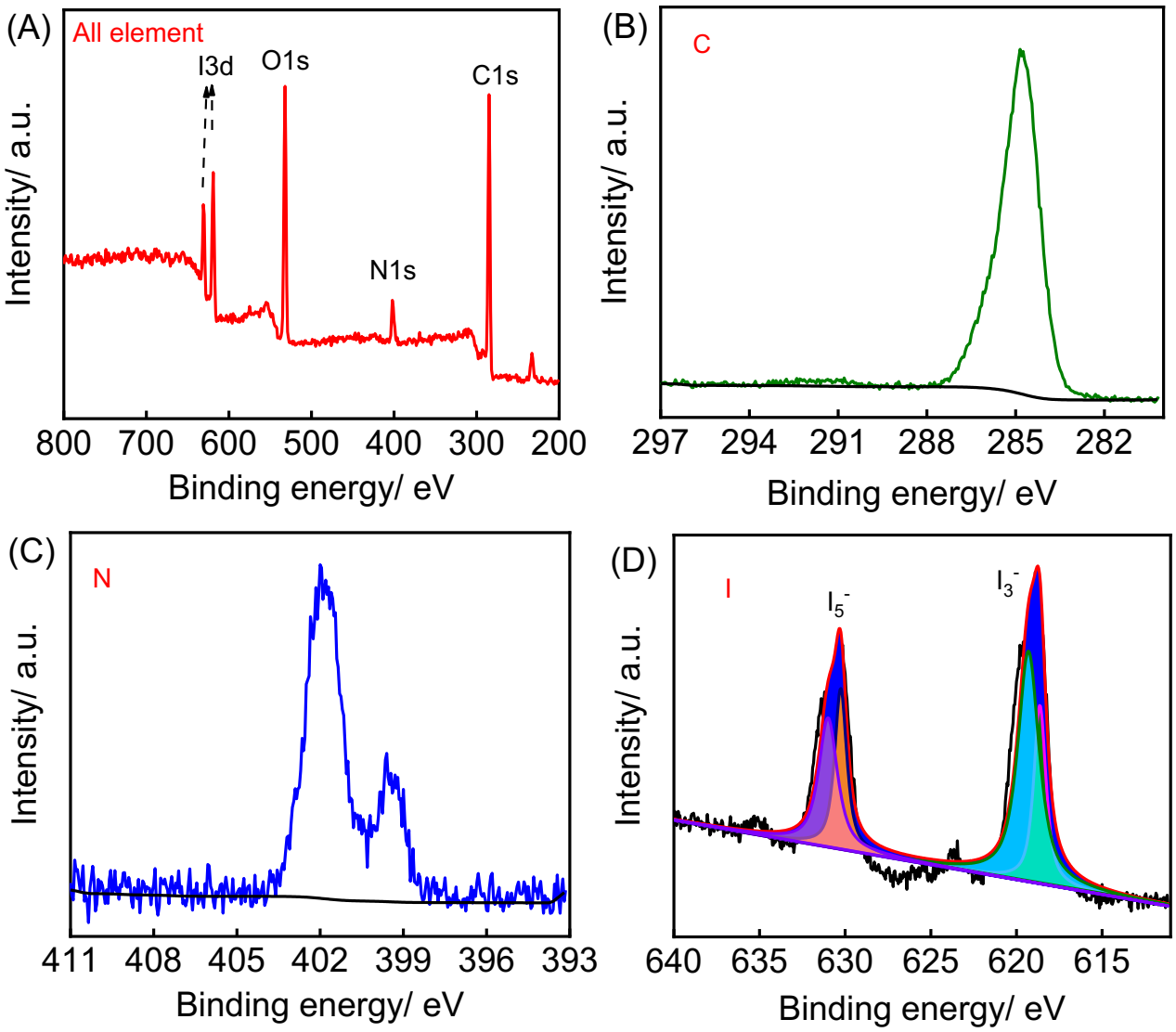

Fig. S49. XPS full spectra of (A) I_2⊂ **PrAn[2]**, (B)C1s, (C)N1s and (D) I3d XPS spectra of I_2⊂ **PrAn[2]**.

6. Iodine uptake experiments in an aqueous solutions

Standard calibration curve

I_2 solution absorbance-concentration standard calibration curve is obtained by measuring the absorbance value at a wavelength of 460nm at different concentrations.

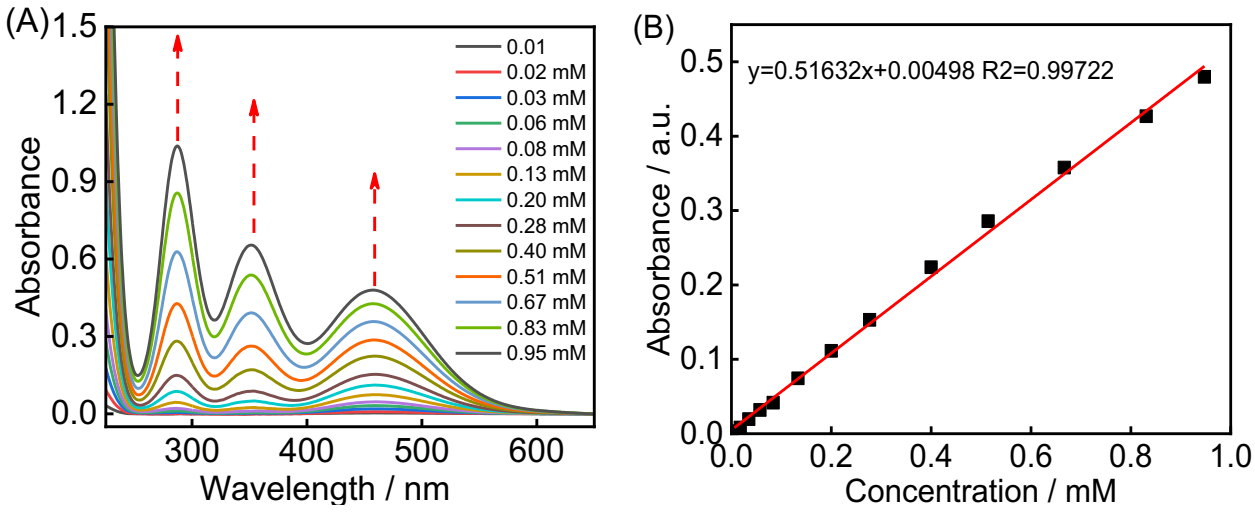

Fig. S50. (A) UV-Vis spectra of aqueous iodine solutions at different concentrations. (B) The standard curve plotted based on the absorbance at 460 nm (right).

Iodine adsorption from the solutions [4]

An[2]s and P-Ns (5 mg) was added into an aqueous iodine solution (1.0 mM, 2.5 mL) and stirred at room temperature. Samples were taken at various time points and filtered. After constructing appropriate calibration curves, the concentration of iodine in the filtrate was determined by UV-Vis spectroscopy. The efficiency of iodine removal (%) by the adsorbents subject to study was determined using following equation:

$$\text{Iodine removal efficiency} = \frac{C_0 - C_t}{C_0} \quad (2)$$

where C_0 (mM) and C_t (mM) are the concentrations of iodine before and after adsorption, respectively.

The amount of adsorbed iodine was determined using the following equation:

$$qt = \frac{(C_0 - C_t) \times Mw \times V}{1000m} \times 100\% \quad (3)$$

where qt (g g^{-1}) is amount of iodine adsorbed per g of adsorbent at time t (min). C_0 (mM) and C_t (mM) are the initial and residual concentrations of iodine in the stock solution and filtrate, respectively; V(mL) is the Is the volume of iodine solution used for adsorption; m(g) is the mass of adsorbent used in the study. Mw (g mol^{-1}) is the molar mass of iodine.

Adsorption kinetics

The adsorption kinetics were quantified using Pseudo-second-order model from which the apparent rate constant kobs can be obtained:

$$\frac{t}{q_t} = \frac{1}{k_2 q_e^2} + \frac{t}{q_e} \quad (4)$$

where qt and qe are the adsorbate uptakes (g adsorbate per g An[2]s) at time t (min) and at equilibrium, respectively, and kobs is an apparent second-order rate constant (g g−1 min−1). The rate constant kobs can be calculated from the intercept and slope of the plot of t/qt against t.

Table S6. Kinetic data corresponding to iodine adsorption by the An[2]s (2 mg mL^{-1}) of this study from the aqueous iodine source phase (1.0 mM).

Entry	Slope	Intercept	q_e	k_{obs}	R^2
				g g^{-1} min^{-1}	
MeAn[2]	6.8981	4.6722	0.1450	10.1844	0.9980
EtAn[2]	6.4385	0.9436	0.1553	43.9320	0.9995
PrAn[2]	6.5677	1.3789	0.1530	31.2820	0.9999
P-A	6.4767	0.3671	0.1533	114.2676	0.9999
P-B	6.5224	0.1814	0.1529	234.5187	0.9999
P-C	6.5304	0.2794	0.1530	152.6346	0.9999
Acs[5]	6.5774	290.6384	0.152	0.1490	0.9960

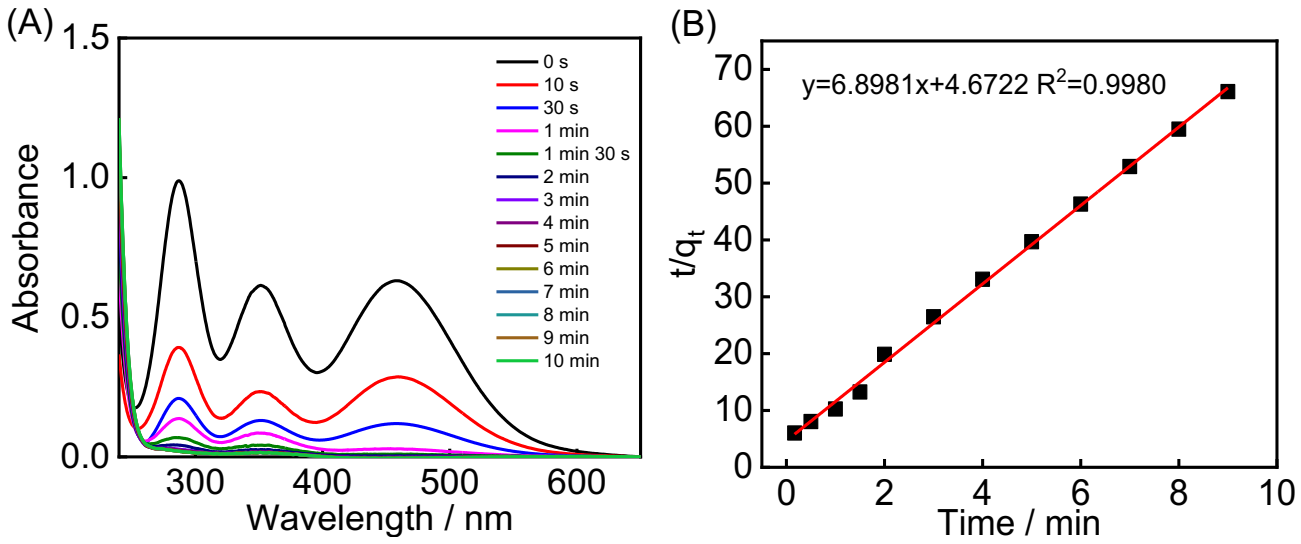

Fig. S51. (A) Time-dependent UV/vis absorption spectra of aqueous I_2 solution (1.0 mM) upon stirring in the presence of **MeAn[2]** (5.0 mg). (B) Line fitting with Pseudo-second-order models for adsorption kinetics data.

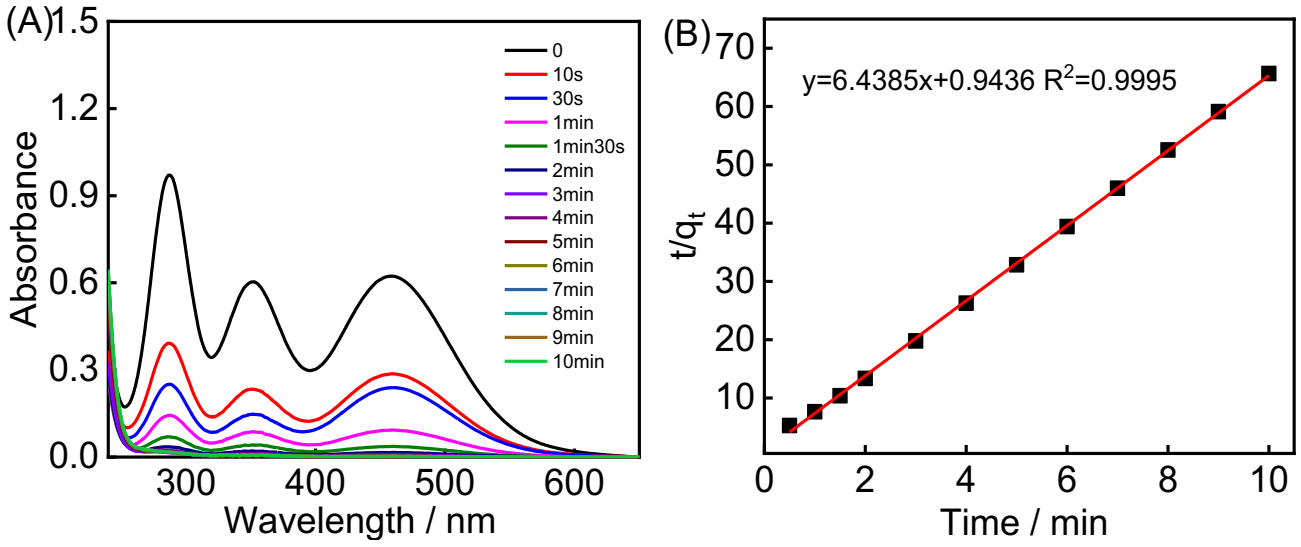

Fig. S52. (A) Time-dependent UV/vis absorption spectra of aqueous I_2 solution (1.0 mM) upon stirring in the presence of **EtAn[2]** (5.0 mg). (B) Linear fitting following the Pseudo-second-order model based on the adsorption kinetics data.

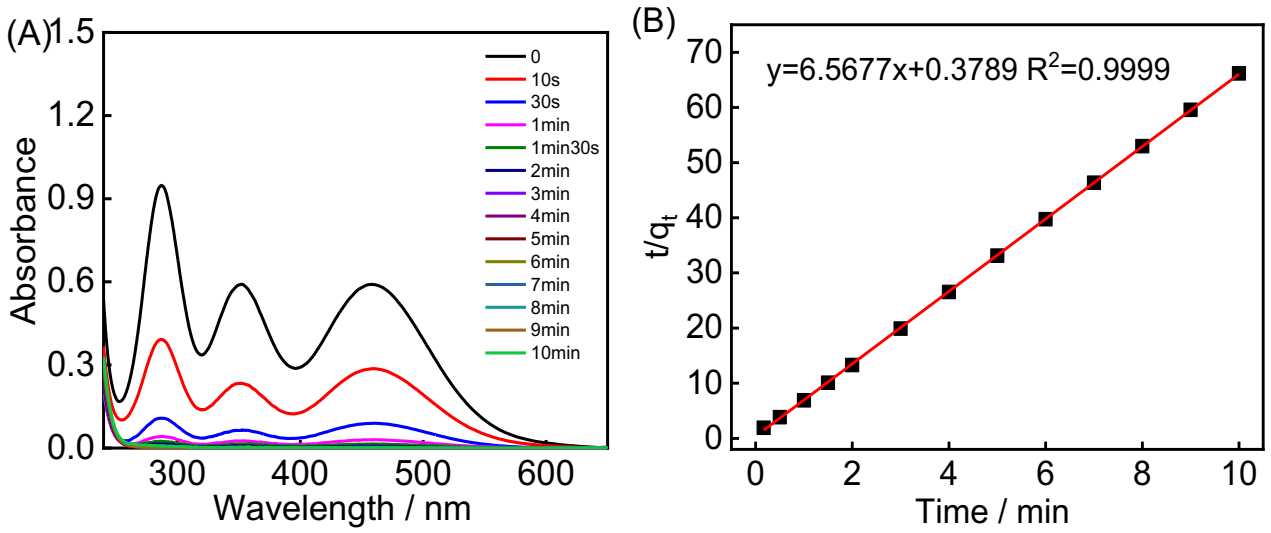

Fig. S53. (A) Time-dependent UV/vis absorption spectra of aqueous I_2 solution (1.0 mM) upon stirring in the presence of **PrAn[2]** (5.0 mg). (B) Linear fitting following the Pseudo-second-order model based on the adsorption kinetics data.

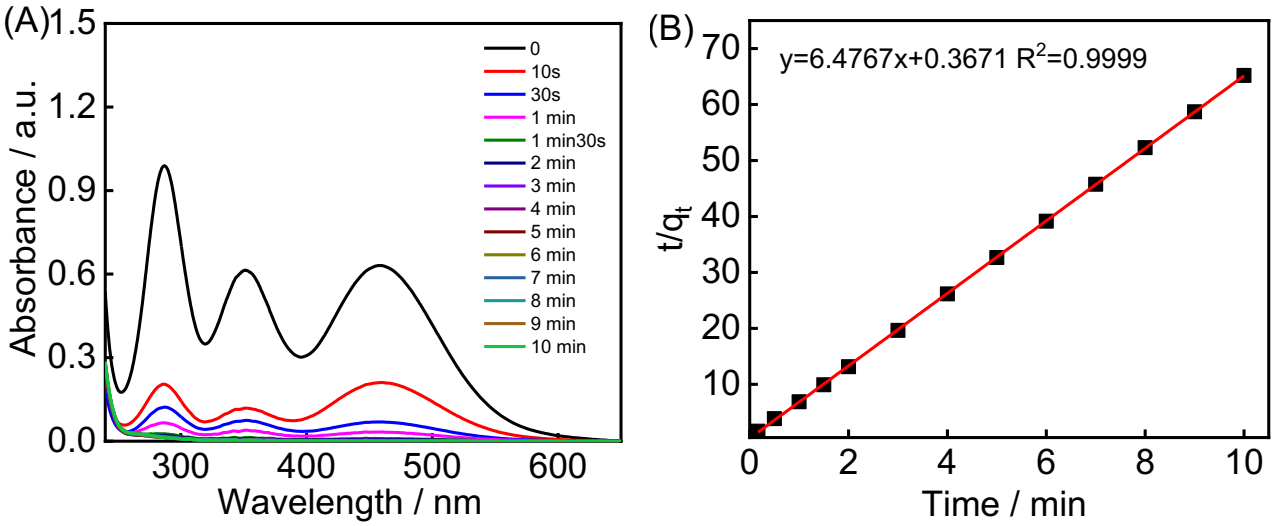

Fig. S54. (A) Time-dependent UV/vis absorption spectra of aqueous I_2 solution (1.0 mM) upon stirring in the presence of **P-A** (5.0 mg). (B) Line fitting with Pseudo-second-order models for adsorption kinetics data.

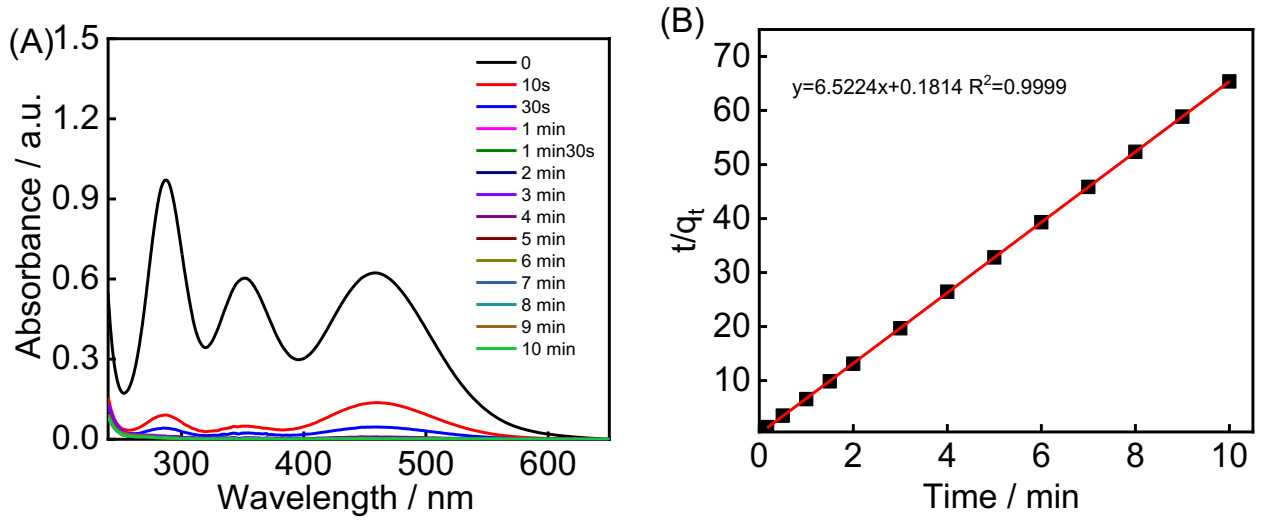

Fig. S55. (A) Time-dependent UV/vis absorption spectra of aqueous I_2 solution (1.0 mM) upon stirring in the presence of **P-B** (5.0 mg). (B) Line fitting with Pseudo-second-order models for adsorption kinetics data.

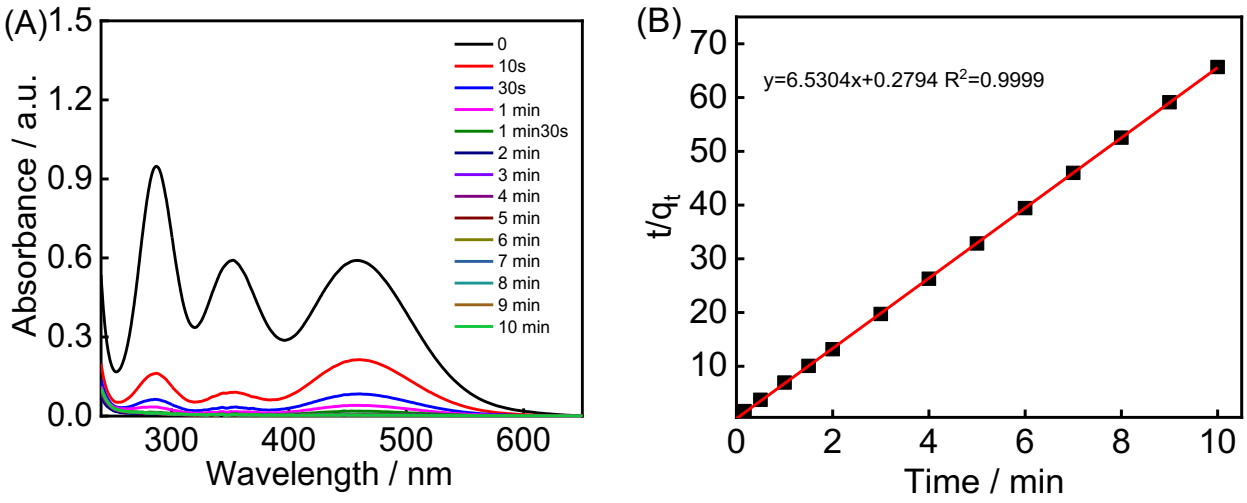

Fig. S56. (A) Time-dependent UV/vis absorption spectra of aqueous I_2 solution (1.0 mM) upon stirring in the presence of **P-C** (5.0 mg). (B) Line fitting with Pseudo-second-order models for adsorption kinetics data.

Table S7. The ratio of I_2 to **An[2]**s

	Mw g/mol	q_m g/g	Calculation formula
A[a]	M[b]	q[c]	$\frac{q}{Mw_I} \div \frac{1}{M}$
MeAn[2]	600.3291	5.28	$\frac{5.28}{253.8} \div \frac{1}{600.3291} = 12.49$
EtAn[2]	656.3905	7.35	$\frac{7.35}{253.8} \div \frac{1}{656.3905} = 19.01$
PrAn[2]	712.3437	7.01	$\frac{7.01}{253.8} \div \frac{1}{712.3437} = 19.68$

[a]name; [b]relative molecular mass; [c]adsorption capacity.

Table S8. The charge balance of I_2 to **An[2]**s based on the peak area of the XPS spectrum

	$A_{630\ eV}$(I_5^-)[a]	$A_{619\ eV}$(I_3^-)[b]	$\frac{A_{630\ eV}}{A_{619\ eV}}$	Contents of Iodine species	N_I
MeAn[2]	8675.483	13100.400	2:3	3 I_5^- &4.5 I_3^-	28.5
EtAn[2]	7506.148	12226.700	2:3	4 I_5^- &6 I_3^-	38
PrAn[2]	10017.52	16022.54	2:3	4 I_5^- &6 I_3^-	38

[a]The peak area of binding energy at 630 eV; [b]The peak area of binding energy at 619 eV.

Table S9. Comparison of iodine adsorption capacities in the aqueous solution of various adsorbents.

Materials	**Iodine uptake Capacity (g g-1)**	**Type**	**Reference**
MeAn[2]	5.48	Anilino macrocycle	This work
EtAn[2]	4.40	Anilino macrocycle	This work
PrAn[2]	3.80	Anilino macrocycle	This work
P-A	3.34	Aniline-based polymer	This work
C[4]P-BTP	3.24	Calix[4]pyrrole	Angew. Chem. 2021, 133, 2–10
P-B	3.10	Aniline-based polymer	This work
CaCOP3	3.1	Calix[4]arenes	Mater. Chem. Phys.,2020, 239, 122328
C[4]P-TPE	2.99	Calix[4]pyrrole	Angew. Chem. 2021, 133, 2–10
CaCOP2	2.81	Calix[4]arenes	Mater. Chem. Phys.,2020, 239, 122328
P-C	2.56	Aniline-based polymer	This work
CaCOP1	2.4	Calix[4]arenes	Mater. Chem. Phys.,2020, 239, 122328
CalCOP1	2.32	Polycalix[4]arenes	J Mater Sci., 2020, 55, 1854
HCOF-1	2.1±0.1	HOF	*J. Am. Chem. Soc.* 2017, 139, 7172
CalCOP2	1.758	Polycalix[4]arenes	J Mater Sci., 2020, 55, 1854
3D MOF-1	1.1±0.05	MOF	*ACS Appl. Mater. Interfaces.,* 2020, 12, 46107
TAPB-BPDA	0.988	Nitrogen-containing COF	*React Funct Polym.,* 2021, 159, 104806
THPS-C	0.926	Triptycene	*Adv. Mater. Interfaces.*, 2019, 6, 1900249
CalCOP3	0.346	Polycalix[4]arenes	J Mater Sci., 2020, 55, 1854
CalCOP4	0.156	Polycalix[4]arenes	J Mater Sci., 2020, 55, 1854
G-QP6	0.247	Quaterphen[n]arenes	Angew. Chem. Int. Ed. 2019, 58, 3885
G-QP5	0.245	Quaterphen[n]arenes	Angew. Chem. Int. Ed. 2019, 58, 3885
G-TP5	0.243	Terphen[n]arenes	Angew. Chem. Int. Ed. 2019, 58, 3885
G-TP6	0.24	Terphen[n]arenes	Angew. Chem. Int. Ed. 2019, 58, 3885
DTTP5	0.0943	Pillar[5]arene-based	Polym. Chem., 2021,12, 3517

7. Fixed bed adsorption experiment

A column with a cross-sectional area of 20 mm^2 was filled with **An[2]**s (50 mg). A saturated aqueous iodine solution (1.2 mM, 10 mL) was then passed through this column at a flow rate of 0.6 mL min^{-1} as controlled by a syringe pump. The eluent was analyzed directly by means of UV/Vis spectroscopy.

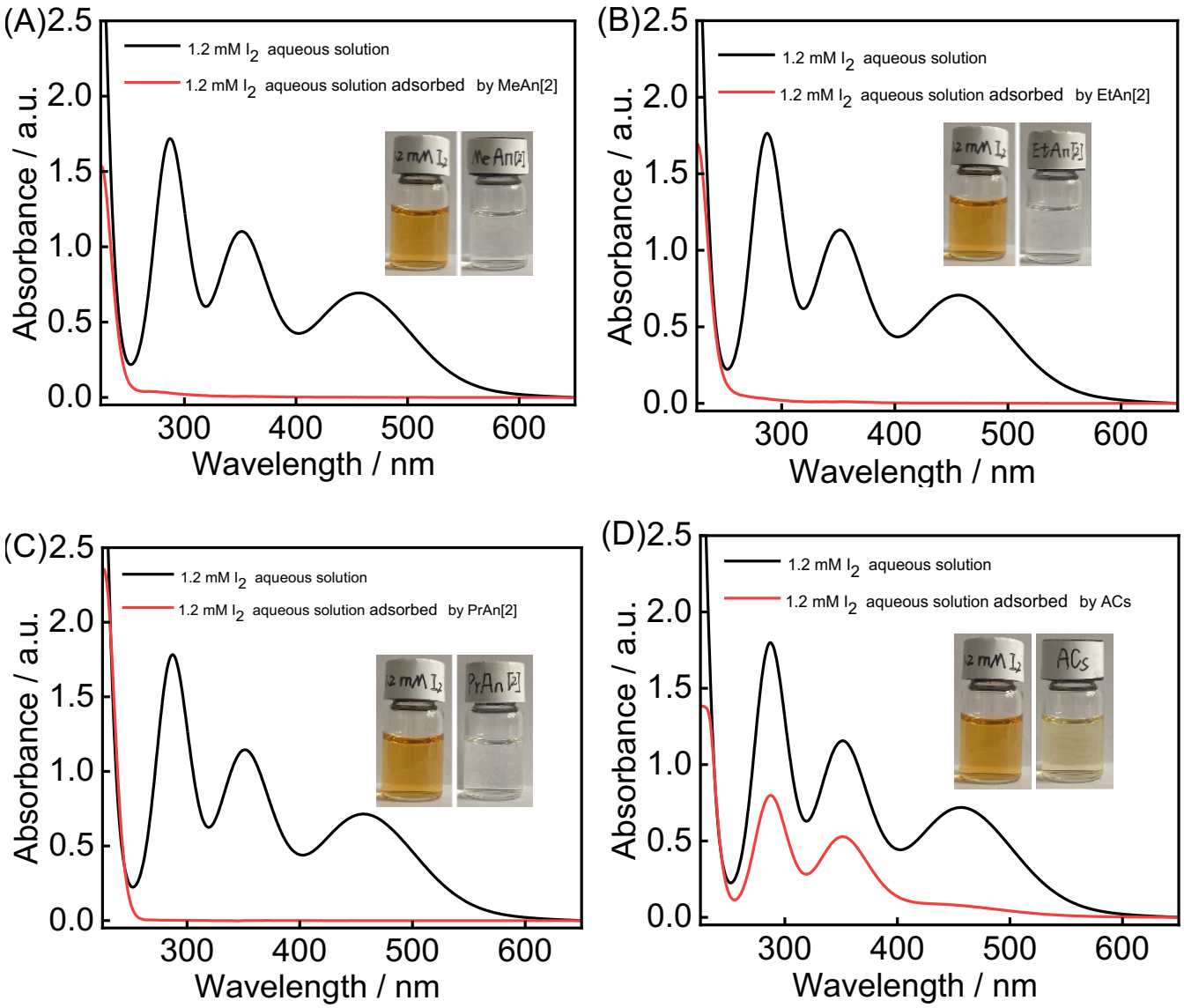

Fig. S57. UV/Vis spectra of saturated iodine aqueous solutions before and after flow-through adsorption by (A-C) **An[2]**s and (D) activated carbons (ACs), respectively. The inset shows the color changes of the iodine aqueous solution after flow-through adsorption by **An[2]**s and ACs, respectively.

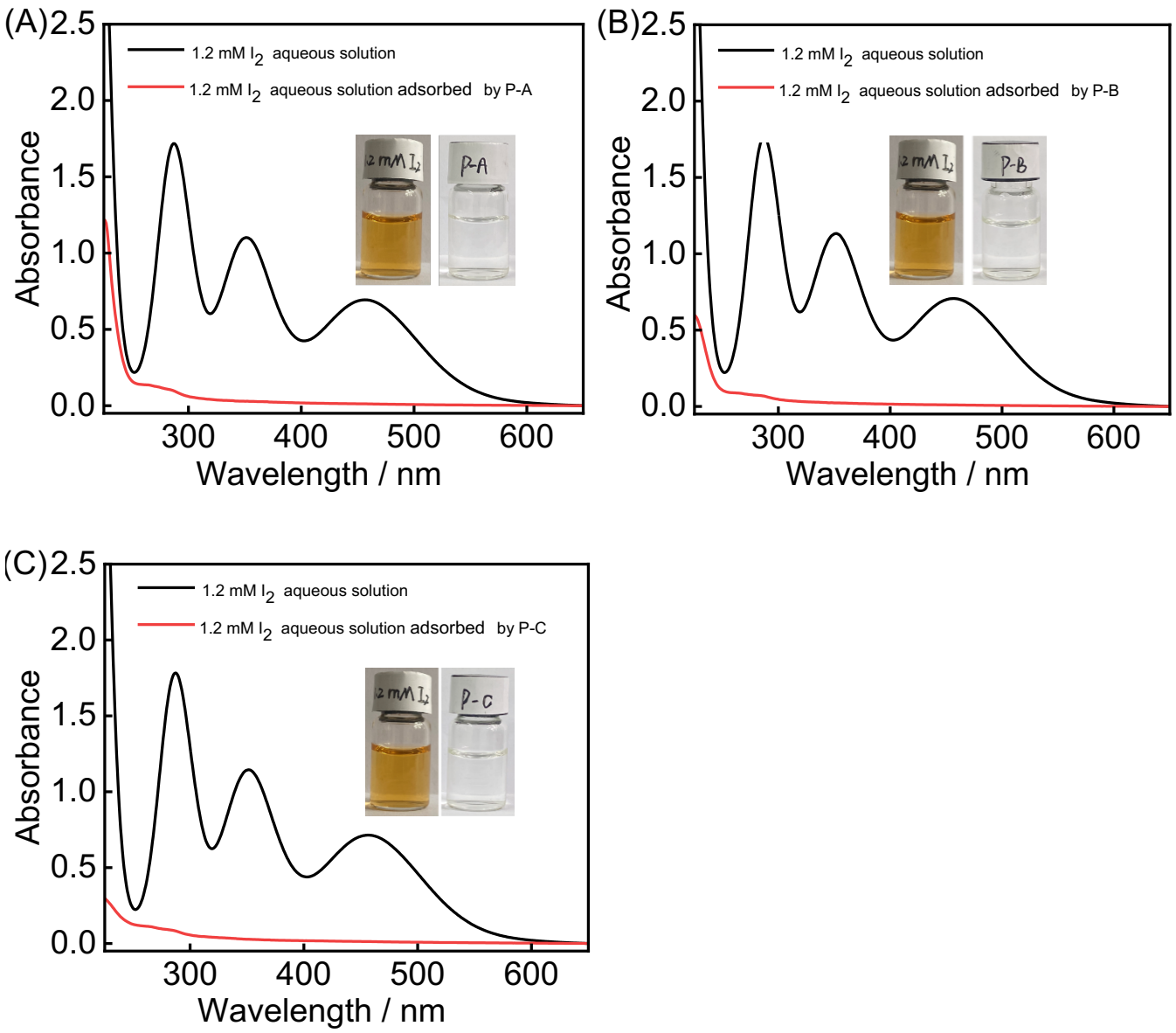

Fig. S58. UV/Vis spectra of saturated iodine aqueous solutions before and after flow-through adsorption by **An[2]**s's polymers. The inset shows the color changes of the iodine aqueous solution after flow-through adsorption by the polymers, respectively.

8. Iodine release

Iodine release from iodine-loaded An[2]s

In order to monitor the iodine-releasing speed from iodine-loaded macrocyclic arenes, time-dependent UV/vis spectral measurements were carried out in cyclohexane. In a typical experiment, an iodine-loaded macrocycle was immersed in cyclohexane. in a vial with stirring. The UV-Vis adsorptions were recorded by periodically withdrawing a 10 mL cyclohexane solution from the mother solution and transferring it back after the spectral measurement.

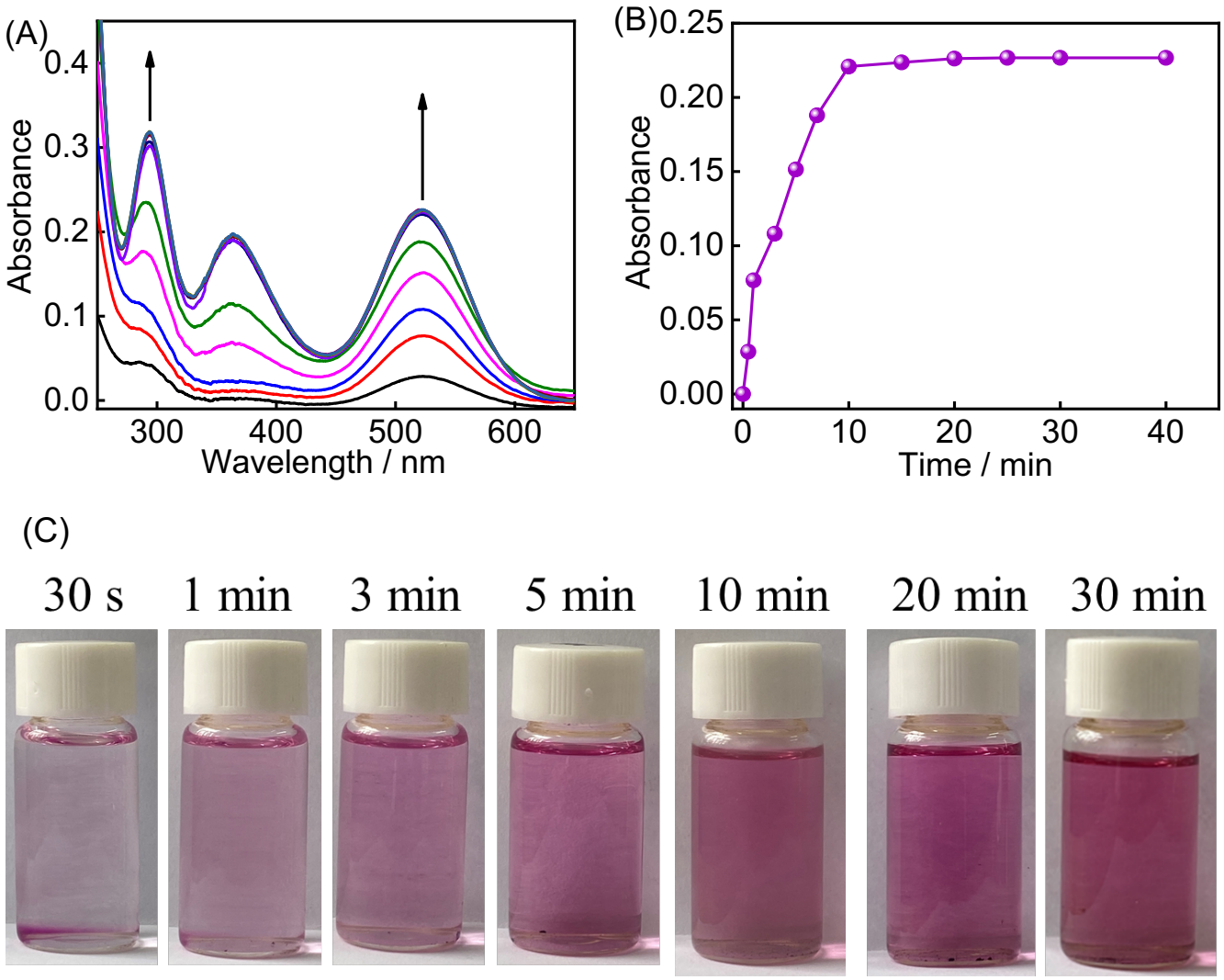

Fig. S59. (A) Time-dependent UV/vis spectral changes after adding 0.5 mg I_2⊂ **MeAn[2]** in 10.0 mL cyclohexane. B) I_2 absorbance at 522 nm at various times in (A). (C) Photographs of iodine release of 0.5 mg I_2⊂ **MeAn[2]** in 10.0 mL cyclohexane.

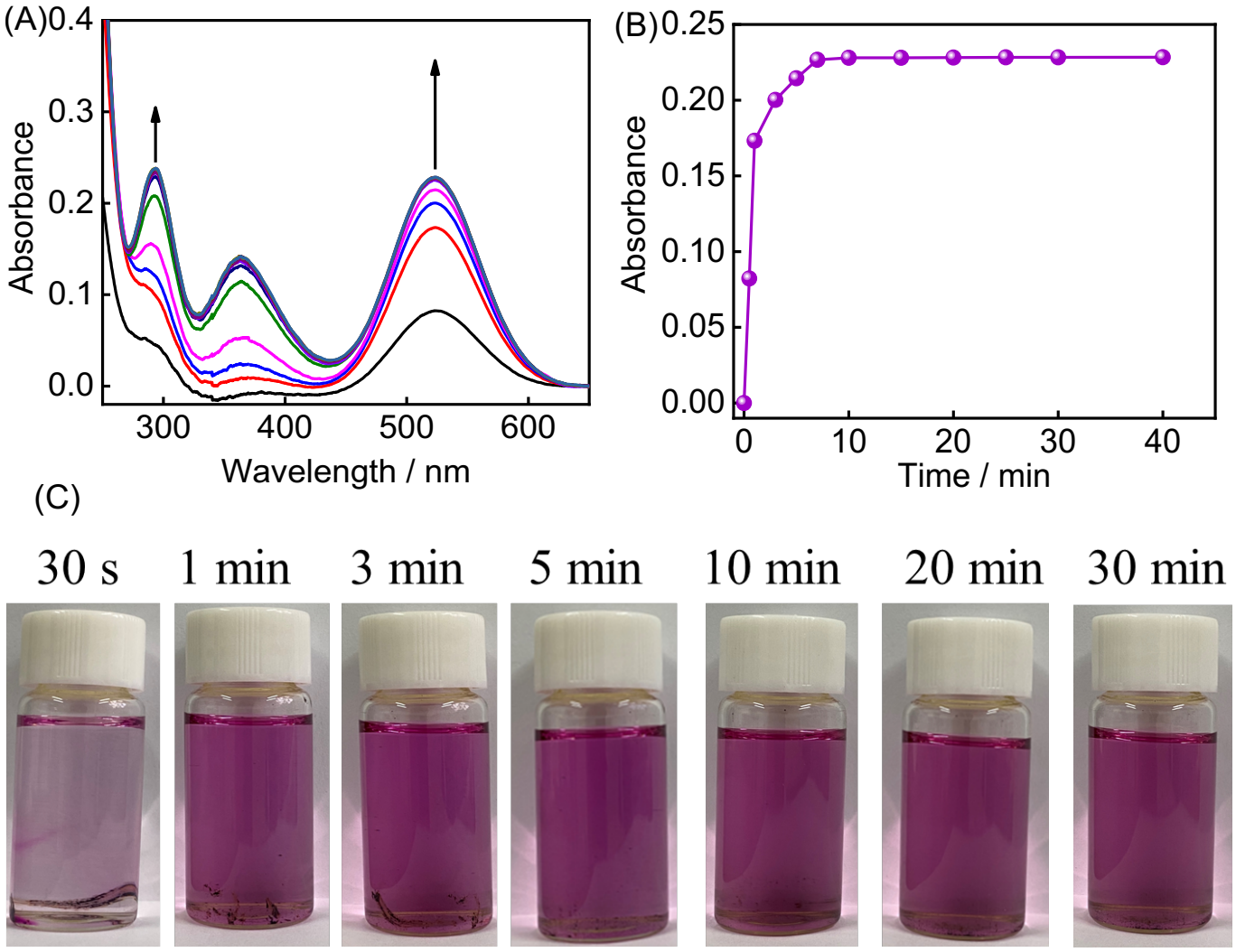

Fig. S60. (A) Time-dependent UV/vis spectral changes after adding 0.5 mg I_2⊂ **PrAn[2]** in 10.0 mL cyclohexane. (B) I_2 absorbance at 522 nm at various times in (A). (C) Photographs of iodine release of 0.5 mg I_2⊂**PrAn[2]** in 10.0 mL cyclohexane.

Field emission scanning electron microscope(FESEM) of I_2⊂ MeAn[2] after the release of iodine

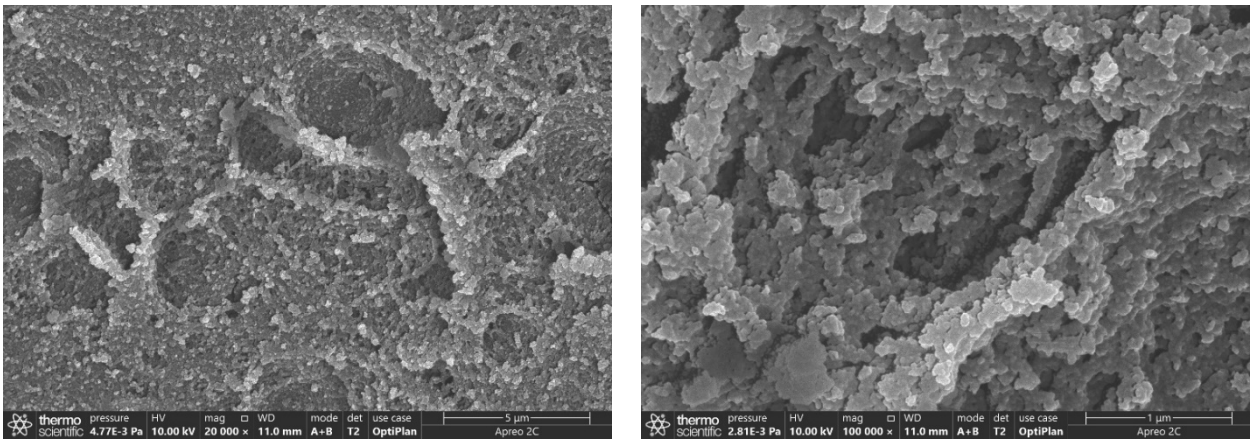

Fig. S61. Scanning electron microscopy images of I_2⊂ **MeAn[2]** after the release of iodine

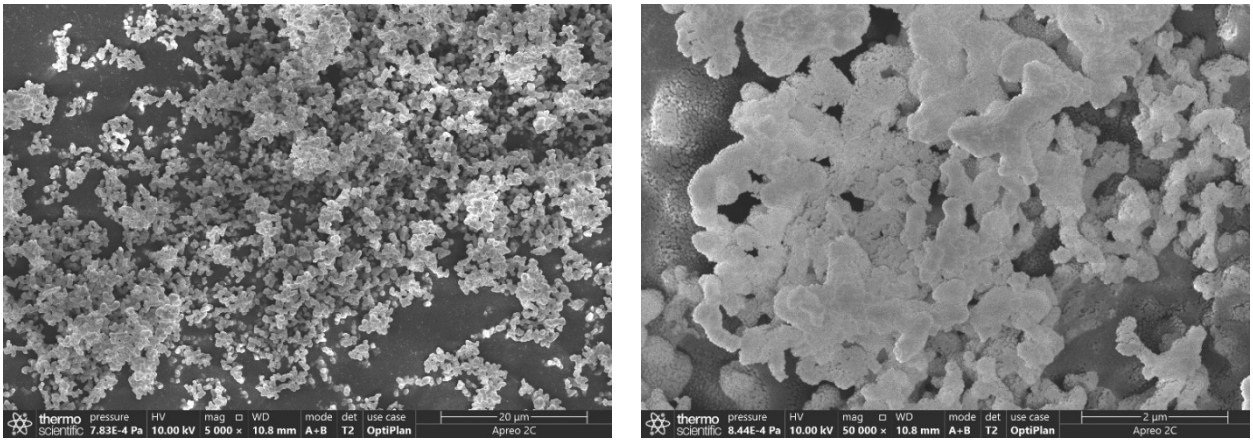

Fig. S62.Scanning electron microscopy images of I_2⊂**EtAn[2]** after the release of iodine

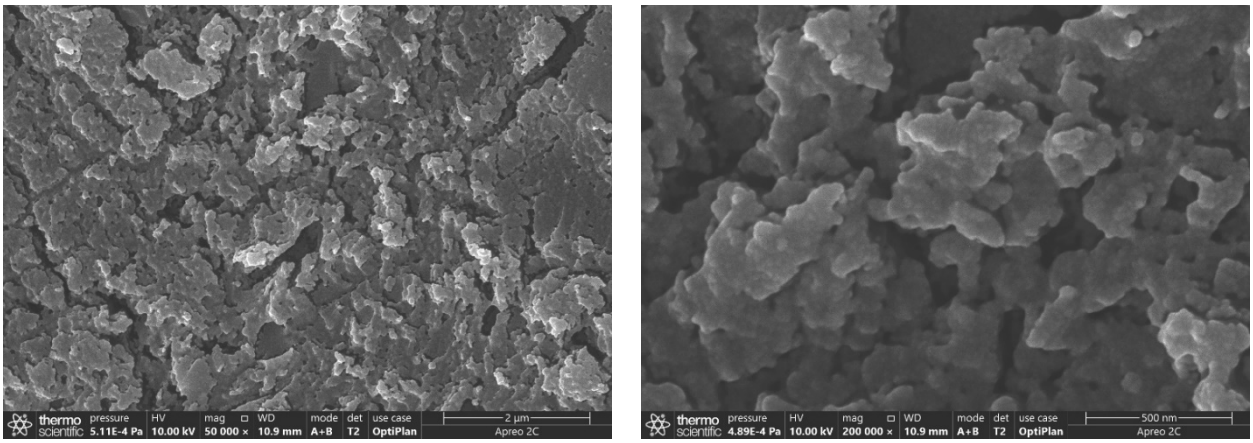

Fig. S63.Scanning electron microscopy images of I_2⊂ **PrAn[2]** after the release of iodin

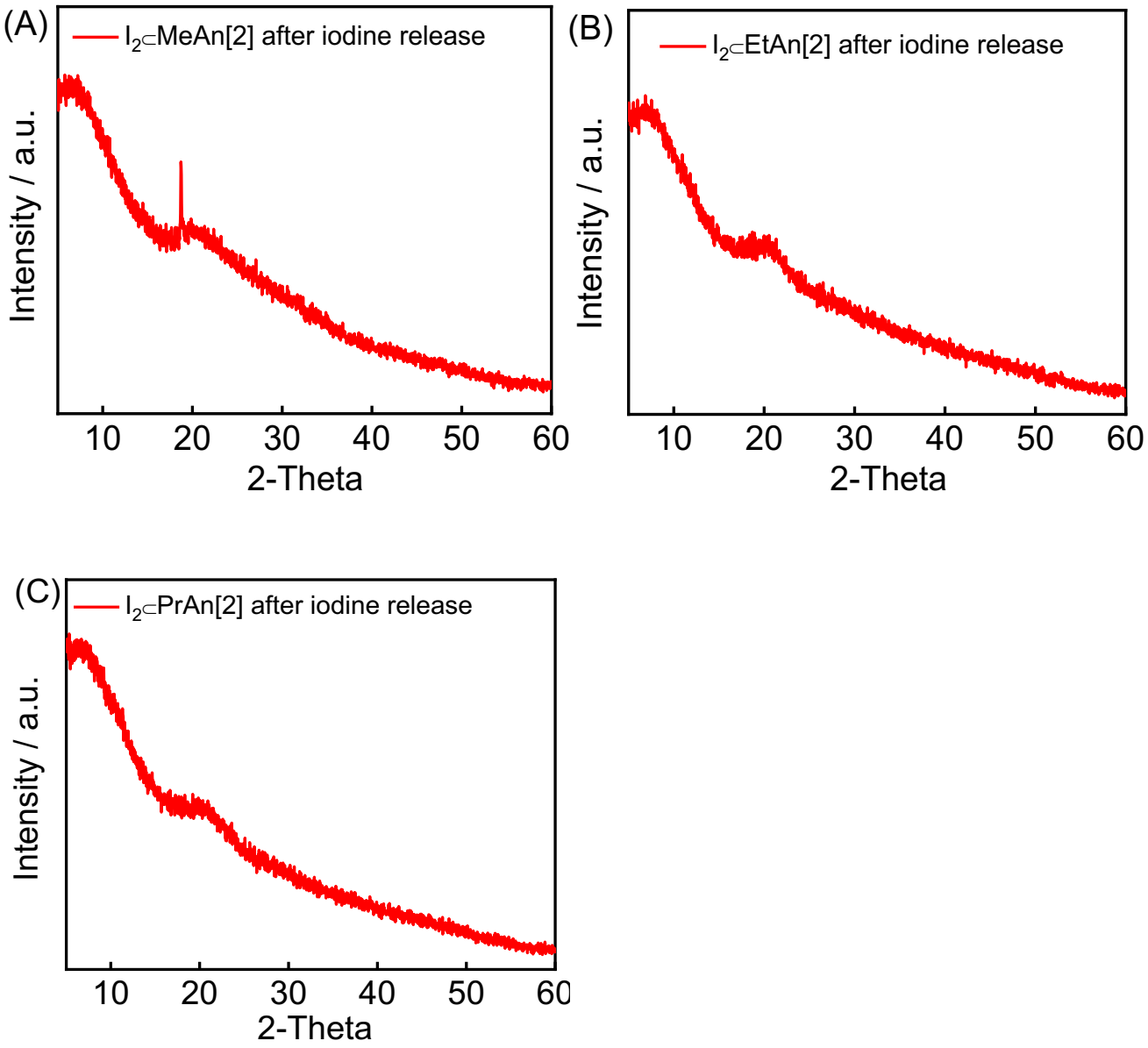

Fig. S64. X-ray powder diffractogram of (A) **MeAn[2]** ,(B) **EtAn[2]** and (C) **PrAn[2]** after iodine release.

9. Selectivity and Reproducibility study

In the selectivity experiment, 5 mg of An[2]s or P-Ns was immersed into a binary solution which containing 5 mL of I_2 solution (1 mM) and each of various interference anions solution (NO_3^-, Cl^-, $CH3COO^-$, Br^-, SO_4^{2-}, and F^-) (1 M). For 24h, the final mixture was stirred at room temperature and filtered. The concentration of iodine in the filtrate was determined by UV-Vis spectroscopy. Blank solution and mixed solution represent I_2 solution (1 mM) with no or all competing ions, respectively.The efficiency of iodine removal (%) by the adsorbents subject to study was determined using equation (2):

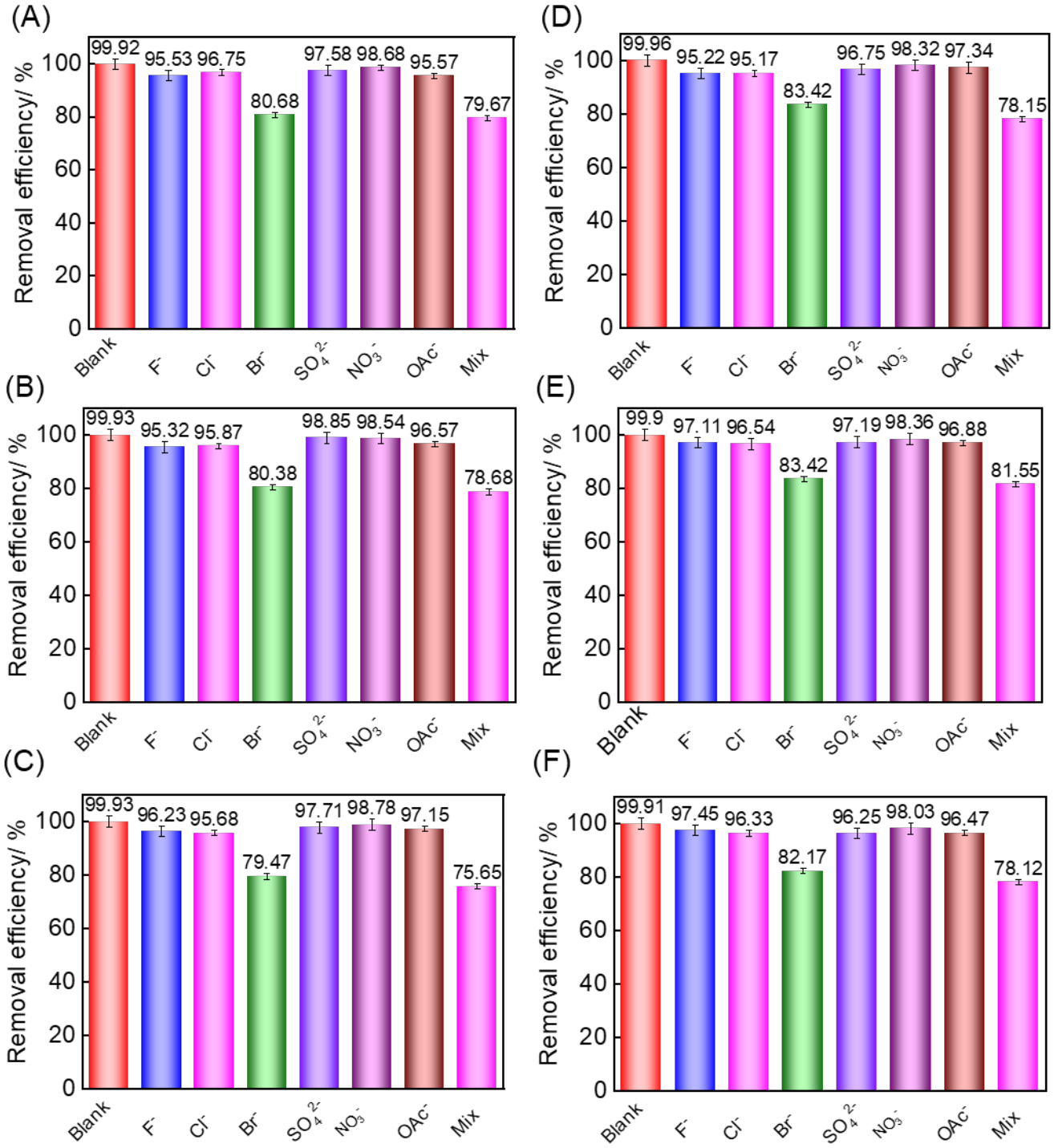

Fig. S65. The removal efficiency of aqueous I_2 solution (1.0 mM) by (A)MeAn[2], (B) EtAn[2], (C) PrAn[2], (D)P-A, (E)P-B, and (F)P-C in the presence of no, a single or all interference ions.

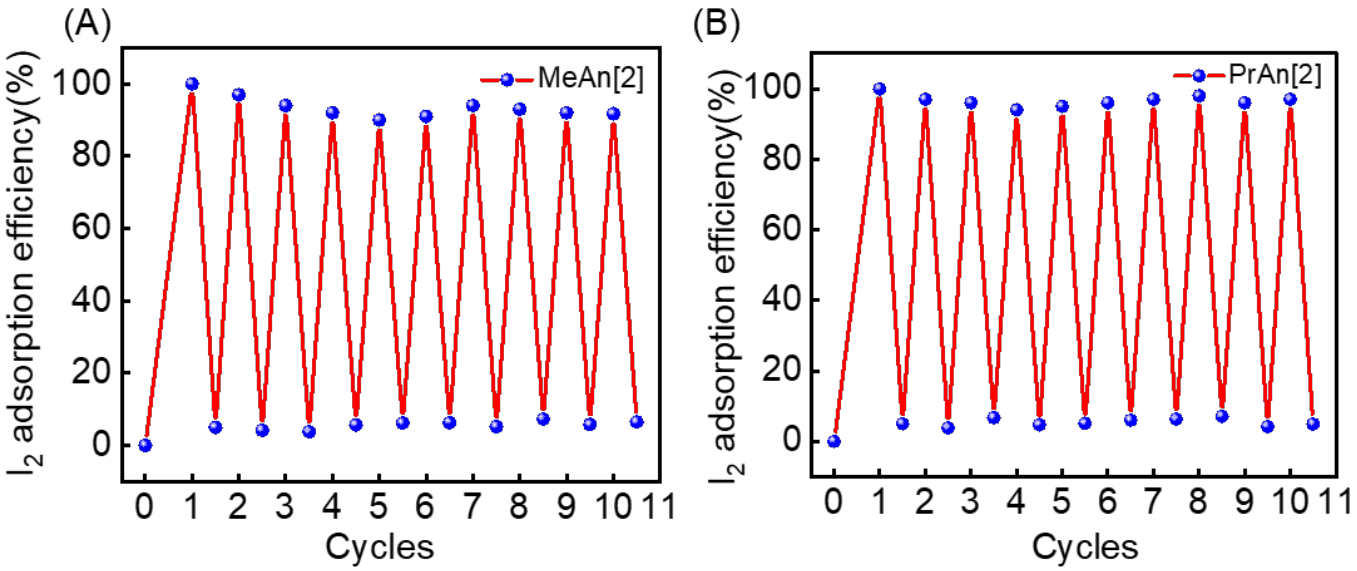

Fig. S66.Recycling performance of **MeAn[2]** and **PrAn[2]**.

10. References

1 P. J. Stephens, F. J. Devlin, C. F. Chabalowski and M. J. Frisch, *J. Phys. Chem.*, 1994, **98**, 11623–11627.

2 P. C. Hariharan and J. A. Pople, *Theoret. Chim. Acta*, 1973, **28**, 213–222.

3 E. Laviron, *Journal of Electroanalytical Chemistry and Interfacial Electrochemistry*, 1979, **100**, 263–270.

4 X. Yu, W. Wu, D. Zhou, D. Su, Z. Zhong and C. Yang, *CCS Chem.*, , DOI:10.31635/ccschem.021.202101036.

5 L. Xie, Z. Zheng, Q. Lin, H. Zhou, X. Ji, J. L. Sessler and H. Wang, *Angew. Chem. Int. Ed.*, 2021, **134**, e202113724.